Multi-Omic Atlas reveals cytotoxic phenotype and ROS-linked metabolic quiescence as key features of CTL-resistant HIV-infected CD4$^+$ T-cells

Alberto Herrera*[1,2], Louise Leyre*[1,2], Jared Weiler[1], Noemi Luise Linden[1,2], Tan Thinh Huynh[1], Feng Wang[1], Colin Kovacs[3], Marina Caskey[4], Paul Zumbo[5], Maider Astorkia Amiama[5], Sandra Terry[1], Ya-Chi Ho[6], Doron Betel[5], R. Brad Jones[1,2]

[1] Infectious Disease Division, Department of Medicine, Weill Cornell Medicine, New York, NY, USA.
[2] Immunology and Microbial Pathogenesis Program, Weill Cornell Graduate School of Medical Sciences, New York, NY, USA.
[3]Maple Leaf Medical Clinic and Division of Infectious Diseases, Department of Medicine, University of Toronto, Toronto, Canada.
[4]Laboratory of Molecular Immunology, The Rockefeller University, New York, New York, USA.
[5]Applied Bioinformatics Core, Weill Cornell Medicine, New York, NY, USA.
[6]Department of Microbial Pathogenesis, Yale University School of Medicine, New Haven, CT 06519, USA.

*These authors contributed equally.
To whom correspondence should be addressed:
R. Brad Jones
413 E 69th St
New York, NY 10021
Phone: 646-962-4652
rbjones@med.cornell.edu

Summary

Cytotoxic T-lymphocytes (CTL) exert sustained pressure on reservoirs of HIV-infected cells that persist through years of antiretroviral therapy (ART). This selects for latently infected cells, but also potentially for cells that express HIV but possess intrinsic CTL resistance. We demonstrate that such resistance exists in HIV-infected CD4$^+$ T-cells that survive rigorous CTL attack and map CTL susceptibility to cell identities and states defined by single-cell multi-omics and functional metabolic profiling. Cytotoxic CD4$^+$ T-cells were prominently overrepresented amongst survivors, as were cells with quiescent metabolic profiles and low levels of reactive oxygen species (ROS) production. The induction of ROS production by treatment with deferoxamine sensitized these cells to CTL-mediated elimination. Reservoir-harboring cells from clinical samples share the above transcriptional features, being enriched for quiescent states. Our results provide an atlas for elucidating features of CTL resistance in HIV reservoirs, and identify oxidative stress as a therapeutic target to facilitate reservoir elimination.

Keywords

HIV persistence; cytotoxic T-cells; HIV cure; metabolomics; oxidative stress; immunotherapy

INTRODUCTION

HIV, although manageable as a chronic condition, currently lacks a safe or scalable cure. Antiretroviral therapy (ART) effectively suppresses HIV replication, preventing disease progression and transmission to sexual partners. However, ART does not affect established 'reservoirs', which are rare cell populations harboring integrated, intact proviruses that can reignite viral replication if ART is discontinued[1-3]. A critical reservoir exists in memory CD4$^+$ T-cells, which become increasingly clonal over time due to infected cell proliferation[4-6]. These clonal dynamics

61 facilitate Darwinian selection, favoring reservoir-harboring cells that exhibit fitness advantages in
62 the evasion of immune effectors, including HIV-specific cytotoxic T-lymphocytes (CTL)[7-12].
63 One key mechanism enabling these reservoir-harboring cells to evade CTL clearance is
64 viral latency[1,13]. Amongst intact proviruses, those harbored in genomic locations or orientations
65 that hinder viral transcription increasingly dominate over time on ART[10,14]. Latency is not
66 complete, however. Cells expressing low to moderate levels of HIV RNA can be detected after
67 decades of treatment, as can low levels of HIV p24 protein in blood plasma[15,16]. Associations
68 between virologic measures of HIV persistence and HIV-specific T-cells frequencies and functions
69 suggest ongoing CTL recognition of infected cells[17-21].
70 Two main mechanisms likely contribute to the persistence of HIV-expressing cells despite
71 ongoing CTL surveillance. First, clonal expansion of HIV-infected $CD4^+$ T-cells on ART
72 replenishes fractions of the population that express antigen and are cleared[22-24]. Second, some
73 infected $CD4^+$ T-cells may be intrinsically resistant to CTL attack, mirroring a phenomenon
74 observed in cancer (reviewed in [25]). Overexpression of the anti-apoptotic factor BCL-2 has been
75 identified as one mechanism of CTL resistance[26-28]. The BCL-2 antagonist ABT-199 sensitizes
76 HIV reservoir-harboring cells to CTL elimination *ex vivo* and is currently being investigated in a
77 clinical trial[26] (NCT05668026). Multi-omic profiling of *ex vivo* HIV reservoir-harboring cells has
78 identified other potential mechanisms of CTL resistance, including the granzyme B inhibitor
79 SERPINB9, and the immune checkpoint ligand PVR (CD155)[12,22,29]. However, understanding the
80 contribution of these and other factors to HIV persistence has been limited by the lack of a
81 reference profile of CTL-resistant, HIV-infected $CD4^+$ T-cells.
82 In this study, we confirm the existence of HIV-expressing primary $CD4^+$ T-cells that can
83 survive repeated CTL attacks. We then characterize their transcriptomic and surface protein
84 profiles at the single-cell level, providing a valuable reference for reservoir characterization
85 studies. Furthermore, we uncover how metabolic and oxidative stress features influence the
86 susceptibilities of these cells to CTL attack and show that an FDA-approved drug can be

87 leveraged to boost the elimination of HIV-infected cells *in vitro*. This work shifts the paradigm on
88 HIV persistence and opens novel therapeutic avenues for curing infection.
89
90 **RESULTS**
91 **A rare population of HIV-expressing memory CD4$^+$ T-cells resists repeated CTL attacks**
92 CD4$^+$ T-cells are highly diverse with respect to both their maturational (e.g. naive versus
93 memory) and polarization (e.g. Th_1 versus Th_{17}) profiles. While it would be of interest to study how
94 intrinsic susceptibility to CTL varies as a function of these parameters, we reasoned that
95 mechanistic drivers of resistance were more likely to be revealed by their fluctuations and
96 selection within a relatively homogenous starting population. We therefore adapted a method of
97 activating and culturing naïve CD4$^+$ T-cells under non-polarizing conditions to foster a central
98 memory T-cell (T_{CM}) phenotype, which we infect with HIV during the activation process (Figures
99 1A, S1A and S1C-D)[30,31]. To enable rigorous evaluation of specific CTL killing, we developed a 2-
100 virus system where cells are infected with either a wild-type (WT) clinical isolate strain of HIV,
101 'HIV_{JRSCF}' (targets)[32], or a version of this same virus with a single escape mutation in the TW10-
102 Gag epitope, $HIV_{JRSCF\ TW10esc}$ (bystanders), preventing recognition of the epitope by TW10-specific
103 CTL clones generated from the peripheral blood of people living with HIV (PLWH) (Figures S1B
104 and S1E).
105 We first assessed whether a CTL resistant population exists within these infected T_{CM},
106 using a 'sequential killing assay'. Infected T_{CM} were generated using PBMCs from two HLA-
107 B57$^+$A02$^+$ people without HIV. Cells infected with either WT HIV_{JRSCF} (targets) or $HIV_{JRSCF\ TW10esc}$
108 (bystanders) were stained with different dyes, mixed together and co-cultured with an HLA-B57-
109 restricted CTL clone targeting the Gag 'TSTLQEQIGW' (TW10) epitope for 16 hours (Figures 1A
110 and S1D-S1E). This design ensures that both infected populations experience the same milieu,
111 which is important since factors such as IFN-γ can alter susceptibility to CTL killing (e.g. by
112 upregulating MHC-I)[33]. As expected, $HIV_{JRSCF\ TW10esc}$ -infected cells (bystanders) were only

113 minimally affected by the presence of the TW10-specific CTL clone, while WT HIV_{JRSCF} -infected
114 cells (targets) were mostly eliminated (approximately 90% of initial HIV-Gag^{+} cells) (Figures 1B
115 and 1C). A small population of targeted cells, however, survived this initial CTL attack (10% of
116 initial HIV-Gag^{+} cells) (Figures 1B and 1C). To determine whether this rare population of surviving
117 targets was intrinsically resistant to CTL killing, we performed a second round of CTL co-culture,
118 where now WT HIV_{JRSCF}-infected survivors and $HIV_{JRSCF\ TW10esc}$-infected bystanders were both
119 subject to attack. This was achieved by removing the TW10-specific CTLs from the first round of
120 killing and co-culturing the infected cells with an HLA-A02-restricted, SL9-Gag-specific CTL clone
121 (Figure 1A). The SL9-specific CTLs efficiently eliminated the $HIV_{JRSCF\ TW10esc}$-infected cells that
122 had been bystanders in the first round of killing, indicating efficient cytotoxic effector function.
123 Critically, however, the WT HIV_{JRSCF}-infected cells that had been targeted and survived in the first
124 round, were not further reduced by the SL9-specific CTL attack (Figures 1B and 1C). This
125 provides direct evidence for the presence of rare populations of HIV antigen-expressing CD4^{+} T-
126 cells that are intrinsically resistant to CTL-mediated killing.

127 **Distinct clusters of CTL-resistant cells identified by multi-omic profiling**

128 Having confirmed the ability of this *in vitro* system to identify *bona fide* CTL resistant cells,
129 we next characterized the transcriptional profiles, the surface expression of 140 immunologic
130 markers, and the clonotypic identities of rare CTL-resistant survivors compared to bystanders
131 using Extended CRISPR Compatible Cellular Indexing of Transcriptomes and Epitopes by
132 Sequencing (ECCITE-seq)[34,35] (Figures 1D and 1E). For both populations, we sorted cells based
133 on HIV-Env expression to isolate cells that survived despite antigen expression, versus selecting
134 for latently infected cells (Figure 1D). Harmony-based integration of ECCITE-seq data from 4
135 donors, followed by Weighted Nearest Neighbor (WNN) analysis of integrated gene expression
136 and surface protein profiles revealed 11 different unsupervised clusters among total HIV-
137 expressing T-cells. Strikingly, CTL-resistant survivors were specifically enriched in 4 of the 11
138 clusters; clusters 2, 4, 9 and 11 (Figure 1F and Table S1). In breaking down the skewing of

139 survivors and bystanders in these clusters by donor, we observed that 3/4, 2/4, 4/4 and 3/4 donors
140 showed enrichment of survivors versus bystanders in clusters 2 (average 2.5-fold enrichment), 4
141 (average 3-fold enrichment), 9 (average 3.9-fold enrichment) and 11 (average 3.6-fold
142 enrichment) respectively (Figure 1G and Table S1).

143 Conversely, certain clusters of infected cells were highly sensitive to elimination (skewed
144 towards bystanders). These were clusters: 0 (1.9-fold reduction), 1 (2.0 fold-reduction), 5 (1.9-
145 fold reduction), 6 (5.3-fold reduction), and 7 (1.5-fold reduction) with skewing observed in 4/4, 2/4,
146 2/4, 4/4 and 3/4 donors respectively (Figure 1G and Table S1). While we also leveraged TCR
147 sequencing to consider whether particular T-cell clones varied in their susceptibilities to killing,
148 we observed very little in the way of expanded clones in either the bystander or survivor
149 populations (Figure S2A). This is unsurprising given that our model uses polyclonal activation of
150 naïve CD4 T-cells, with limited time for clonal expansion.

151 **An atlas of transcriptional features defining CTL-resistant or susceptible clusters**

152 To probe for transcriptional programs that may contribute to CTL resistance or sensitivity
153 in the cells making up survivor- and bystander-enriched clusters, we identified the top differentially
154 expressed genes in each cluster and performed pathway enrichment analysis. Amongst the CTL-
155 resistant clusters, we identified a cytotoxic signature and high expression of adhesion genes in
156 cluster 9, high expression of ribosomal proteins in cluster 2, and an interferon stimulated gene
157 (ISG) signature/high antiviral response in cluster 4 (Figure 2A and 2B). Conversely, amongst CTL-
158 sensitive clusters, we identified high expression of activation and stress genes in cluster 0;
159 activation and metabolic genes in cluster 1; activation, proliferation and adhesion genes in
160 clusters 5 and 6, and cell division genes in cluster 7. Clusters 3 and 10 were omitted from further
161 analysis due to their cells expressing a disproportionately high percentage of mitochondrial genes
162 compared to other clusters, indicating these were lower quality/pre-apoptotic cells (Figure S2B).

163 To further define the identifies of bystander- and survivor-enriched clusters, we leveraged
164 an independent dataset defining activation status and functionality modules in T-cells and overlaid

165 these on our WNN-defined clusters[36]. We scored the levels of gene expression from infected cells
166 on modules from this reference dataset descriptive of activation profiles: “Treg-like activation” and
167 “Proliferation”; an intermediate activation module: “IFN response”; cytotoxicity profiles: “CD8
168 cytotoxicity” and “CD8 cytokines”; and a resting “naïve/T_{CM} $CD4^+$ T-cells” profiles. In line with our
169 previous analysis, CTL-sensitive clusters 0, 1, 5, 6 and 7 had the highest expression of modules
170 highly associated with activation, such as the “Treg-like activation” module in clusters 0, 1, 5 and
171 6, and the “proliferation” module in clusters 0 and 7 (Figures 2C and S2C-S2D). For CTL-resistant
172 clusters, cluster 4 had high expression of “resting naïve/T_{CM} $CD4^+$ T-cells” as well as the “IFN
173 response” modules, while cluster 9 scored markedly high for the “CD8 cytotoxicity” and "CD8
174 cytokine” modules (Figures 2C and S2E-S2H). These results demonstrated a tendency for cells
175 with higher activation and proliferation profiles to readily succumb to killing by CTL, while cells
176 enriched for resting, IFN response and cytotoxic profiles tended to be resistant to CTL.

177 In addition to host genes, we assessed levels of HIV transcription in relation to the CTL
178 susceptibilities of cell clusters. Since cells had been sorted for those expressing HIV-Env,
179 essentially all cells contained readily detectable levels of HIV transcripts. While CTL-resistant
180 clusters 2 and 4 neither showed lower basal levels of HIV transcripts than susceptible clusters in
181 the unselected bystanders, nor selection for the lower end of this distribution amongst survivors,
182 cytotoxic cluster 9 stood out in having significantly lower levels of HIV transcripts than other
183 clusters - manifesting as a bi-modal distribution of HIV-transcript-high versus HIV-transcript-low,
184 and the latter was moderately enriched amongst the survivors of CTL selection (Figures 2D-2E).
185 Thus, overall, levels of HIV expression did not appear to be a major determinant of CTL
186 susceptibility (in the context of our model of sorted HIV-Env^+ cells). However, relatively low levels
187 of HIV expression might contribute to CTL evasion in a subpopulation of cytotoxic HIV-infected
188 $CD4^+$ T-cells.

189 Our results indicate that amongst infected cells generated in a cultured T_{CM} system we
190 can capture diversity in cellular and immunophenotypic modules associated with both resistance

191 and susceptibility to CTLs. The strongest transcriptional predictor of CTL-susceptibility in HIV-
192 expressing CD4$^+$ T-cells appears to be high expression of activation and proliferation programs,
193 while CTL-resistant cells were enriched for multiple cellular states including IFN responses and
194 engagement of a cytotoxicity program.

195 **CTL resistance in HIV-expressing cells is linked to quiescent transcriptional and**
196 **immunophenotypic states**

197 To pan-out to the most widely shared cellular features delineating CTL-resistant survivor
198 cells from bystanders, we next performed differential gene expression and pathway enrichment
199 analysis on all survivor cells compared against all bystander cells, across the 4 donors. Amongst
200 the genes with the most reduced expression levels in survivors were those coding for TNF-
201 receptor superfamily member costimulatory receptors *TNFRSF18* (GITR), *TNFRSF4* (OX40) and
202 *TNFRSF9* (4-1BB), the chemokine receptor *CXCR3*, the dual specificity phosphatase *DUSP4* and
203 the metallothionine *MT2A* – all transcripts expressed downstream of T-cell activation[37-39] (Figure
204 3A and Table S2). Pathway enrichment analysis revealed that several aerobic metabolism-related
205 gene-sets were the most downregulated in survivor cells (Figure 3B). Relatedly, oxidative stress
206 (KEAP1-NERF2) as well as proliferation (cell cycle) gene-sets were robustly down in these cells
207 compared to bystanders. As T-cell activation induces a shift towards aerobic glycolysis and heavy
208 reliance on glucose oxidation to sustain clonal expansion, termed the Warburg effect[40], we
209 proceeded to quantify the extent to which genes along the glucose metabolism cascade were
210 differentially expressed. We calculated module scores in single cells based on their individual
211 expression levels of genes annotated as members of each pathway subtracted by aggregate
212 control features[41]. Our analysis revealed significant downregulation in survivor cells of glycolysis,
213 aerobic respiration, and oxidative phosphorylation pathways as well as other general metabolism
214 sets (Figure 3C and S3A-S3D). Oxidative stress, arising from the production of reactive oxygen
215 species (ROS) as a natural consequence of active metabolism[42,43], was found to be reduced in
216 survivors based on our pathway enrichment analysis, which revealed downregulation of genes

217 involved in the oxidative stress response (Figure 3B). Accordingly, module scoring of ROS and
218 and oxidative stress response pathways revealed concomitant downregulation of their gene-sets
219 in survivor cells (Figure 3C), indicating that lower activation thresholds in survivors translated to
220 a more quiescent-like transcriptional program in these cells with reduced levels of oxidative stress
221 responses.

222 To assess if the immunophenotypes of CTL-resistant survivor cells followed the course of
223 their transcriptional states, we quantified surface protein expression of markers of T-cell
224 activation/differentiation and function in our ECCITE-seq data. Our analysis revealed 2-fold and
225 1.5-fold downregulation of the early activation markers CD69 and CD71 (the transferrin receptor)
226 (Figure 3D). Similarly, other activation induced markers including Fas, PD-1, CD5, CD7, CD44
227 and the costimulatory receptors CD28, 4-1BB and OX40 were markedly down in survivors
228 compared to bystander cells (Figure 3D). Activation induced integrins CD54 (ICAM), CD2, CD57
229 and CD49a, important for the stabilization of immune synapses with CTLs, were also robustly
230 down in survivor cells (Figure 3E). Conversely, resting markers were upregulated in survivor cells
231 compared to bystanders, including the adhesion molecule CD62-L (L-selectin) highly expressed
232 in naïve and resting central memory T-cells (Figure 3F). These results highlight an enrichment of
233 transcriptional programs denoting metabolic quiescence and redox balance, as well as a resting
234 immunophenotypic state, as the most widely shared features of HIV-expressing cells that survive
235 CTL attack.

236 **CTL-resistant, HIV-expressing cells have reduced levels of metabolic flux and oxidative**
237 **stress**

238 Since transcriptional and surface protein profiling of HIV-expressing survivor cells
239 implicated quiescence and reduced oxidative stress, we next evaluated the bioenergetic demand
240 and dependency of these cells via Single Cell ENergetIc metabolism by profilIng Translation
241 inHibition (SCENITH)[44]. This method measures puromycin incorporation as a readout for new
242 protein translation to measure the bioenergetic capacity of single cells through flow cytometry.

243 The use of different metabolic inhibitors targeting separate arms of ATP production allows for the
244 deconvolution of glucose dependence (using OXPHOS inhibition) and mitochondrial dependence
245 (using glycolysis inhibition). SCENITH analysis of HIV-expressing survivors revealed 1.22-fold
246 and 1.25-fold lower levels of new protein translation compared to non-targeted bystander HIV-
247 expressing cells in the same culture and HIV-expressing cells in the absence of CTL pressure,
248 respectively (Figure 4A). This lower bioenergetic capacity in survivor cells was mainly attributed
249 to reduced dependency on glucose oxidation, as survivors exhibited similar reductions in new
250 protein translation when OXPHOS was inhibited, and did not show differences in translation
251 compared to bystanders and infected cells without CTL pressure when glucose oxidation alone
252 or both processes were inhibited (Figure 4B). These results confirmed that CTL-resistant, HIV-
253 expressing survivors are enriched for cells with overall lower levels of metabolic flux compared to
254 non-targeted HIV-expressing cells and that this reduced bioenergetic capacity is a result of lower
255 glucose metabolism.

256 Since our preliminary transcriptomics data indicated that CTL resistant survivors have
257 dual downregulation of metabolic and oxidative stress gene-sets (Figures 3B and 3C), we
258 reasoned that survivor cells may exhibit decreased intracellular ROS. To address this, we coupled
259 our killing assay readouts with flow cytometry-based detection of intracellular ROS accumulation
260 using CellROX green and $DCFH_2$-DA[45,46]. These are compounds that become highly fluorescent
261 when oxidized following reactions with a wide array of reactive oxygen species. Analysis of ROS
262 accumulation in infected cells cultured with or without CTLs revealed that the presence of CTLs
263 led to an increase in ROS accumulation in both survivor and bystander HIV-expressing cells
264 compared to HIV-expressing cells cultured in the absence of CTLs (Figure 4C), suggesting that
265 the culture microenvironment during a killing assay induces increases in intracellular ROS.
266 Survivor cells, however, showed selection for cells with lower levels of ROS accumulation
267 compared to bystanders in the same wells (Figure 4C), suggesting that ROS hi cells are
268 preferentially susceptible to CTL-mediated death. Notably, survivors were also drastically

269 depleted of cells expressing either CD69 or the transferrin receptor, CD71, responsible for
270 intracellular uptake of iron (Figures 3D and 4D), implying that HIV-expressing cells with lesser
271 activation states have a resistance advantage to CTL attack. An additional arm of cellular stress
272 that culminates in the accumulation of intracellular ROS and metabolic reprogramming is the
273 hypoxic response, which follows cellular activation in immune cells even in the presence of
274 oxygen[47]. The Hallmark hypoxia gene-set as well as direct *HIF-1A* transcript levels from our
275 sequencing analysis were found to be significantly reduced in CTL-resistant survivors compared
276 to bystanders and these reduced levels were also confirmed for HIF1-A at the protein level
277 (Figures 4E, 4F and S3D). Overall, these results demonstrated an enrichment towards metabolic
278 quiescence and reduced oxidative stress in CTL-resistant, HIV-expressing cells. As CTL-derived
279 granzyme A and granzyme B can both induce rapid mitochondrial depolarization and associated
280 increases in intracellular ROS in targeted cells[48,49], our results suggest that superior redox balance
281 by a sub-population of HIV-expressing cells protects them from CTL-mediated elimination.

282 **Pharmacological induction of ROS and hypoxia sensitizes infected cells to CTL-mediated**
283 **elimination**

284 We next sought to address whether manipulating the redox state of HIV-expressing cells
285 with the FDA-approved compound Deferoxamine (DFO) could improve CTL-mediated elimination
286 of these cells. DFO is an iron chelator used for the treatment of excessive iron overload[50] which
287 stabilizes HIF-1a accumulation to induce a hypoxic mimic response and oxidative stress[51-54]. We
288 observed that - in the absence of CTLs - treatment with DFO induced robust intracellular
289 accumulation of ROS in infected cells (Figures 5A). This was complemented by a marked
290 upregulation of CD71 surface expression among DFO-treated cells, an additional feature of CTL-
291 sensitive infected cells (Figures 5B, S4A-B). Of note, DFO treatment also resulted in increased
292 the frequencies of cells expressing HIV-Gag (Figure S4C). However, Despite the increase in initial
293 HIV-expressing cells by DFO treatment before co-culture with CTLs, the same numbers of CTLs
294 added across conditions were still able to eliminate a substantially greater proportion of HIV-

295 expressing cells in the DFO-treated condition as compared to the vehicle control (DMSO),
296 indicating a prominent role of DFO in sensitizing HIV-expressing cells to CTL elimination through
297 mechanisms beyond latency reversal (Figures 5C and 5D). Thus, by reversing key metabolic
298 features linked to CTL resistance, DFO potently sensitized HIV-expressing cells to improved CTL-
299 mediated elimination. These results support the induction of ROS buildup in infected targets as a
300 mechanism used by CTL to eliminate these cells and also highlight the ability of DFO to not only
301 induce ROS but also additional arms of oxidative stress, such as the intracellular iron uptake
302 transporter CD71, which can synergize to sensitize targeted cells to CTL-mediated elimination by
303 engaging reactive oxygen- and reactive iron-based cell death pathways (Figure 5E)[48,49,55].

304 **Reservoir-harboring cells that express HIV RNA exhibit CTL resistance metabolic features**

305 Having identified and functionally validated a link between a transcriptional signature
306 denoting quiescence and redox balance to CTL-resistance, we probed its *in vivo* relevance by
307 asking whether this signature was present in cells harboring the HIV reservoir in ART-treated
308 individuals. We leveraged a published data-set to focus on expanded T-cell clones containing
309 cells found to be actively transcribing HIV RNA *ex vivo* reasoning that CTL resistance is most
310 relevant to this 'active' reservoir than to latently infected cells[22]. We scored expression of
311 metabolic and oxidative stress modules in these cells and observed a marked downregulation of
312 aerobic respiration, glycolysis, OXPHOS, hypoxia and ROS response gene-sets among HIV
313 RNA^{+} T-cell clones compared to HIV RNA- counterparts, highly reminiscent of the profiles of HIV-
314 expressing CD4^{+} T-cells that survived CTL attack *in vitro* (Figures 6A-6C). This suggests that the
315 novel mechanism identified in the current study - of CTL resistance through metabolic quiescence
316 - may contribute to the persistence of HIV-expressing CD4^{+} T-cells *in vivo*.

317 **Support for multiple additional mechanisms of resistance in HIV reservoirs**

318 Advances in understanding the role and mechanisms of CTL-resistance in HIV
319 persistence will be supported through bidirectional synergies between the profiles of CTL-
320 resistant cells provided in the current study and ongoing advances in characterizing *in vivo* HIV

321 reservoirs. Above, we have leveraged this framework to generate and functionally validate a
322 hypothesis, which was then cross-referenced with profiles of *bona fide* reservoirs. Here, we
323 reverse this directionality, examining whether previously proposed mechanisms of CTL
324 resistance, identified through *ex vivo* observations, align with the functionally validated resistant
325 cell profiles revealed by our dataset.

326 BCL-2 overexpression has been established as one mechanism by which HIV-infected
327 $CD4^+$ T-cells can resist CTL and to date is the only validated therapeutic target to improve
328 sensitization of infected cells to CTL elimination[26-28]. In the current study, *BCL2* transcripts were
329 significantly overexpressed in CTL-resistant survivor cells compared to bystander cells with the
330 highest mean expression level found in CTL-resistant cluster 4 (Figures 6D and S5A), further
331 underscoring the relevance of this pathway in immune evasion.

332 Another proposed mechanism of resistance involves the immune checkpoint ligand PVR
333 (CD155), which has been reported to be overexpressed on *ex vivo* $CD4^+$ T-cells harboring intact
334 HIV proviruses. This overexpression was suggested to deliver a 'don't kill me signal' to CTLs,
335 promoting immune evasion. Consistent with this hypothesis, our findings show that PVR
336 expression is elevated in CTL-resistant survivors relative to bystanders, with the highest levels
337 found in cluster 11 (Figures 6E and S5B)[12]. This observation is consistent with the role of PVR as
338 a factor contributing to CTL resistance in reservoir cells.

339 Multiple studies have reported that the HIV reservoirs that persist over time in ART-treated
340 PLWH are preferentially harbored in $CD4^+$ T-cell clones with a cytotoxic profile[22,56]. This has led
341 to the hypothesis that these cells may be equipped with mechanisms to resist cytotoxic effector
342 molecules (e.g. perforin and granzyme) as a means of avoiding self-destruction[16]. We leveraged
343 our survivor/bystander comparison to assess this by defining a gene module based on the
344 overexpressed genes in CTL-resistant cytotoxic cluster 9 (Table S3) and applying this to *ex vivo*
345 HIV RNA^+ and HIV RNA- $CD4^+$ T-cell clones from this previous study. In parallel we also
346 reanalyzed this published data using the "CD8 Cytotoxicity" module from Szabo *et al*., 2019 that

347 we had previously observed to be enriched in CTL-resistant cluster 9[22,36]. These analyses
348 revealed a robust enrichment of both cytotoxic modules on HIV RNA^{+} T-cell clones compared to
349 HIV RNA- T-cell clones (Figures 6F-6G). This strong alignment between reservoir-harboring cells
350 and the CTL-resistant cells in cluster 9 lends support to the hypothesis that resistance to killing
351 contributes to the enrichment of HIV reservoirs in cytotoxic CD4^{+} T-cells.

352 **Single-cell multi-omic profiling reveals complex relationship between MHC-I expression**
353 **and CTL susceptibility**

354 The HIV-Nef protein partially downregulates MHC-I downregulation on the surface of HIV-
355 infected cells as a mechanism of partial immune evasion[57]. Thus, one would predict that cells with
356 the lowest levels of surface MHC-I would be enriched our survivors. While this was observed
357 when all cells were analyzed collectively (Figure S5C), further examination within the context of
358 our WNN-defined clusters revealed a more nuanced landscape. Whereas CTL-resistant clusters
359 2, 4, and 11 have amongst the lowest levels of surface MHC-I, CTL resistant cluster 9 has
360 amongst the highest. Conversely, the highly CTL-susceptible cluster 5 expresses amongst the
361 lowest levels of MHC-I (Fig. S5D). Further, when all cells were divided into low (lower tercile),
362 intermediate (middle tercile), and high (upper tercile) expressors of surface MHC-I, we observed
363 that cells expressing intermediate and high levels of MHC-I were appreciably represented
364 amongst CTL-resistant survivors (Fig. S5E and S5F). Similarly, while *BCL2* was overexpressed
365 and PVR were under-expressed in collective survivors (Figure 6C-6D), cluster-specific analyses
366 uncover extensive diversity in expression levels across clusters that do not necessarily track with
367 overall CTL susceptibility of a given cluster (Figure S5A and S5B), further underscoring the
368 diversity in resistance mechanisms across clusters. These findings reinforce the value of a single-
369 cell multi-omic 'atlas' of CTL resistance by further highlighting its ability to capture known and
370 proposed mechanisms of CTL resistance / immune evasion, while revealing underlying
371 complexities which will foster extensive follow-up studies.

372

373 **DISCUSSION**

374 In this study, we provide direct evidence for the existence of populations of HIV-expressing
375 primary CD4$^+$ T-cells that are capable of surviving rigorous attacks by HIV-specific CTLs. This
376 phenomenon has been postulated previously in order to bridge gaps in the canonical model of
377 HIV persistence - which attributes long-term survival of infected cells to viral latency - with recent
378 observations indicating a degree of ongoing HIV expression and CD8$^+$ T-cell surveillance during
379 ART[12,20-22,58]. However, to our knowledge, direct evidence that HIV-expressing cells can possess
380 resistance to CTL has not previously been presented.

381 One important observation from our study is that cytotoxic CD4$^+$ T-cells that express HIV
382 protein are relatively resistant to killing by CTL, compared to non-cytotoxic CD4$^+$ T-cells. The
383 profiles of these cells show excellent agreement with cytotoxic CD4$^+$ T-cells that multiple studies
384 have shown to disproportionately harbor HIV reservoirs in ART-treated PLWH, in particular those
385 that continue to transcribe HIV[22,56]. Uncovering and counteracting the mechanisms by which these
386 survive stringent CTL attack will require further study. Our results do suggest a potential role for
387 somewhat diminished magnitudes of HIV transcription relative to non-cytotoxic cells, though this
388 does not preclude roles for factors shown to protect other types of cytotoxic cells (e.g. CD8$^+$ T-
389 cells and NK cells) from perforin/granzyme B mediated self-destruction, such as the granzyme B
390 inhibitor SERPINB9[59].

391 In addition to this cytotoxic profile, comprehensive multi-omic profiling and WNN clustering
392 revealed that CTL resistant cells were enriched for resting phenotypes, and IFN response
393 signatures, while CTL-sensitive cells exhibit high activation and proliferation. When all cells were
394 considered collectively, metabolic quiescence and reduced intracellular ROS levels emerged as
395 the most widely shared characteristic of CTL-resistant cells, and were validated as a novel
396 mechanism of immune evasion by HIV-expressing cells. This was evident at the level of pathway
397 enrichment analysis, but also at the level of numerous individual genes and proteins - such as
398 dramatic selection amongst survivors against cells expressing CD69 and CD71. In tandem,

399 multiple previously known or proposed mechanisms of CTL resistance were confirmed or
400 supported by our dataset. These findings suggest that CTL-resistant cells evade immune
401 clearance not through a single pathway but via distinct molecular and cellular programs. This is
402 further supported by our observation that two established mechanisms of CTL resistance - MHC-
403 I downregulation and *BCL2* overexpression - show the expected patterns of selection when all
404 cells were analyzed collectively, but no consistent patterns at the levels of WNN-defined clusters
405 of cells. We therefore propose that the datasets presented in this study serve as a foundational
406 resource for advancing a comprehensive and nuanced understanding of CTL resistance in HIV.

407 To build upon this foundation towards therapeutic strategies, we linked transcriptional
408 signatures of metabolic quiescence to low levels of the metabolic byproduct ROS, and
409 demonstrated that the FDA-approved compound DFO markedly improves CTL-mediated
410 elimination of HIV-infected cells. DFO was selected due to its ability to target multiple facets of
411 resistance observed in survivor cells, by increasing CD71 surface expression and inducing
412 hypoxia which culminates in increased intracellular ROS accumulation[51-54]. ROS exerts toxicity
413 by interacting and damaging different essential macromolecules inside of the cell, including
414 DNA[60]. Indeed, ROS buildup as a result of granzyme-mediated mitochondrial damage has been
415 reported to contribute to cell death following a CTL hit[48,49]. However, ROS can also synergize with
416 increased iron uptake via CD71 to induce the Fenton reaction and ROS/iron- mediated
417 ferroptosis, a mechanism not yet studied in CTL-mediated clearance of infected cells[55]. Whether
418 other compounds such as resveratrol or the FDA-approved drug atovaquone, which directly
419 induce ROS production via disruption of the electron transport chain, can have similar or
420 combinatorial effect with DFO will be of future interest[53,61-63].

421 Our study points to further putative novel modalities of resistance for future exploration.
422 Prominent amongst these was the observation of high levels of interferon stimulated genes
423 amongst survivors - to some extent these overlapped with metabolically quiescent clusters,
424 exemplifying that multiple features of resistance can overlap within populations of cells with similar

425 states. One possibility is that these are cells sensing high levels of CTL-derived IFN-γ after
426 surviving a failed killing attempt. Indeed, increased IFN-γ production by CTLs has been
427 demonstrated in the context of poor and prolonged synapse formation with T-cell and macrophage
428 targets and can have consequences on the inflammatory profile of the targets[64]. Alternatively,
429 high levels of basal IFN responses in populations of HIV-infected $CD4^+$ T-cells may be a driver of
430 resistance. For example, IFN responses can have direct effects on the metabolic states of cells
431 that may impact susceptibility to CTL, such as through IFN-γ-mediated suppression of mTORC1
432 signaling and IFIT1- and IFIT3-mediated reductions in translation capacity[65,66].

433 Importantly, the enrichment for metabolic quiescence and redox balance in CTL-resistant
434 survivors also showed remarkable agreement with the metabolic signatures of rare reservoir-
435 harboring cells studied *ex vivo* from PLWH, specifically with the subset transcribing HIV after
436 antigenic stimulation. This convergence supports the clinical relevance of the mechanisms of CTL
437 resistance defined by our study and provides rationale for novel therapeutic approaches to
438 address HIV persistence. Our observations may also have translational implications outside of
439 the context of HIV. In the context of T-cell lymphoma, enrichment of quiescent signatures has
440 also been observed in metastatic cells that disseminate away from the primary site of malignant
441 transformation, suggesting that immune evasion through immune quiescence may contribute to
442 other pathologies where persistent pathologic $CD4^+$ T-cells are targeted[34,67]. Collectively, we
443 provide an extensive atlas for cross-referencing cellular programs that may affect target cell
444 elimination by CTL and propose metabolic perturbation of reservoir harboring cells as a novel
445 therapeutic approach to advance strategies towards an HIV cure.

446 **Limitations of the Study**

447 A limitation of our study is that the full diversity of $CD4^+$ T-cell differentiation and
448 polarization states is unlikely to be reflected in our cultured T_{CM} target cells. While aiming to
449 generate relatively homogenous target cells was a strategic decision made to increase our ability
450 to uncover core functional drivers of CTL resistance, it may be important to extend this to other

451 target populations - for example, $CD4^+$ T-cells that are intentionally polarized towards T follicular
452 helper or cytotoxic profiles. Some degree of this complexity did, however, emerge in our system
453 - notably, cytotoxic $CD4^+$ T-cells with transcriptional profiles that closely aligned with *ex vivo*
454 reservoir-harboring cytotoxic $CD4^+$ T-cells. There are also limitations in the degree to which
455 encounters with CTL and resulting selection *in vitro* stand-in for those that occur *in vivo* and across
456 various tissues. We stress the importance of identifying convergences between features of
457 survivor cells selected in our system and *bona fide ex vivo* reservoir harboring cells in order to
458 discriminate targets with therapeutic potential.

459 **Acknowledgments**

460 We thank all study participants who devoted time to our research. The following reagents were
461 obtained from the NIH HIV Reagent Program, Division of AIDS, NIAID, NIH: Anti-Human
462 Immunodeficiency Virus (HIV)-1 gp120 Monoclonal Antibody (PGT121) cat # ARP-12343, anti-
463 Human Immunodeficiency Virus (HIV)-1 gp160 Monoclonal Antibody (N6/PGDM1400x10E8) cat
464 # ARP-13390, and JR-CSF Infectious Molecular Clone (pYK-JRCSF) cat # ARP-2708). We
465 acknowledge the Biological Resources Branch Preclinical Repository, National Cancer Institute,
466 for providing IL-2 and IL-15. Research reported in this publication was supported by the National
467 Institutes of Allergy and Infectious Diseases of the National Institutes of Health under Award
468 Numbers UM1AI164565 (R.B.J), R01AI181626 (R.B.J), R01AI176601 (R.B.J), R01AI170245
469 (R.B.J), R01AI165031 (R.B.J), UM1AI164562 (R.B.J), R21AI170246 (R.B.J), and R01AI147845
470 (R.B.J). UM1AI164565 and UM1AI164562 were also supported by the National Institutes of
471 Diabetes and Digestive and Kidney Diseases, the National Institute of Mental Health, the National
472 Institute of Neurological Disorders and Stroke, the National Institute on Drug Abuse, and the
473 National Heart, Lung, and Blood Institute. The content is solely the responsibility of the authors
474 and does not necessarily represent the official views of the National Institutes of Health.

475 **Author contributions.** A.H, L.L and R.B.J. initiated the project and were responsible for
476 experiment design. A.H and L.L performed the majority of experiments with assistance from J.W.,

477 T.T.H., and F.W. in specific assays; M.C. and C.K. were directly involved in patient recruitment,
478 sample collection and study design; A.H., P.Z. and M.A.A. performed the bioinformatic analyses
479 with input from D.B. and R.B.J.; A.H., L.L., and R.B.J. wrote the paper with all authors providing
480 input on the manuscript.

481 **Declaration of interests.** R.B.J declares that he served on the Scientific Advisory Board of ViiV
482 Healthcare Limited and received payment for these services as well reimbursement of travel
483 expenses.

484 **Declaration of generative AI and AI-assisted technologies.** During the preparation of this
485 work, the author(s) used GPT 4.0/OpenAI in order to obtain feedback on and refine writing
486 structure and style. After using this tool or service, the author(s) reviewed and edited the content
487 as needed and take(s) full responsibility for the content of the publication.

488

489 **FIGURE LEGENDS**

490 **Figure 1. Existence and multi-omics profiles of CTL-resistant HIV-expressing CD4$^+$ T-cells.**
491 **(A).** Schematic of 'sequential killing assay', featuring two rounds of killing with CTL clones
492 targeting the Gag-TW10 or Gag-SL9 epitopes. **(B and C**). Representative (**B**) and summary (**C**)
493 flow cytometry data showing frequencies of HIV-infected cells (CD4$^-$, HIV-Gag$^+$) cells from
494 different stages of sequential killing assays. In first-round killing with a Gag-TW10-specific CTL
495 clone the majority of cells infected with WT HIV$_{JRCSF}$ (red) are killed, whereas those infected with
496 escape mutant HIV$_{JRSCF\ TW10esc}$ (blue) are not. In second-round killing, 'bystanders' from the first
497 round (HIV$_{JRSCF\ TW10esc}$) are now efficiently killed whereas 'survivors' HIV$_{JRCSF}$ resist further
498 elimination. Shown in **C** are fold changes in infected (CD4$^-$, HIV-Gag$^+$) cells pre- and post-killing
499 across two donors in technical duplicates. **(D)** Gates used to sort infected cells from bystander
500 and survivor populations for analysis by ECCITE-seq. Populations containing WT HIV$_{JRCSF}$ or
501 HIV$_{JRSCF\ TW10esc}$ were first gated based on CFSE and CTV labeling, respectively (Figure S1F-G).

502 Within each of these, cells actively expressing HIV were identified and sorted based on co-
503 staining with the HIV-Env specific broadly neutralizing antibodies PGT121 and N6-
504 PGDM1400x10E8. **(E)** Harmonized WNN UMAP projections of bystander and survivor cells after
505 CTL exposure from 4 donors clustered using cell-to-cell multimodal neighbors (weighted
506 combination of RNA and surface protein similarities (n = 17,231 cells). Donors 1, 2 and 4 were
507 HIV-negative individuals while donor 3 was a PLWH. **(F**) Proportion of bystander and survivor
508 cells across WNN clusters. >50% indicates preferential resistance to CTL whereas <50%
509 indicates preferential susceptibility. **(G)** Proportion of bystander or survivor cells belonging to each
510 WNN cluster out of total bystander or survivor cells stratified by individual donor.

511 **Figure 2. Single cell atlas of transcriptional features defining CTL-sensitive and CTL-**
512 **resistant states in infected cells. (A)** Heatmap of top 10 differentially expressed genes with a
513 $\log_2$ fold-change difference of at least 0.25 passing min.pct ≥ 0.25 and $P_{adj} < 0.05$ among all WNN
514 clusters highlighting overexpressed genes from CTL sensitive clusters (blue) and CTL-resistant
515 clusters (red). **(B)** Top 5 gene ontology enriched pathways with a false discovery rate of 0.05
516 using gene ontology BP gene-sets using overexpressed genes by each WNN cluster passing the
517 filters described in **(A)**. **(C)** Module scoring of T-cell activation and functional states defined by
518 Szabo *et* al., 2019[36], mapped to WNN clusters. Lower panels indicate that cluster 9 has a cytotoxic
519 profile. **(D)-(E)** Quantification and comparison of HIV transcript expression among clusters. P
520 values of Wilcoxon tests are shown.

521 **Figure 3. Quiescent metabolic and activation profiles are enriched in CTL-resistant**
522 **infected cells. (A)** Heatmap of top 30 differentially expressed genes across total pooled
523 bystander and CTL-resistant survivor infected cells with a $\log_2$ fold-change difference of at least
524 0.1 passing min.pct ≥ 0.1 and $P_{adj} < 0.05$. **(B)** Top 10 differentially enriched Gene Ontology BP
525 (left) and REACTOME (right) pathways from genes-sets passing filters defined in (**A**). **(C)** Module
526 scoring of metabolism and oxidative stress gene-sets, mapped to WNN clusters. **(D)** ECCITE-
527 seq-derived surface expression of selected surface protein activation markers, **(E)** integrins

528 (activation-induced)**,** and **(F)** resting. Expression of selected surface protein and gene-expression
529 resting markers. For **(C)-(F)**, P-values of Wilcoxon tests are shown.

530 **Figure 4. Reduced metabolic flux and oxidative stress in CTL-resistant infected cells.**
531 **(A)-(B)** SCENITH metabolic profiling of cells infected with either $HIV_{JRSCF\ TW10esc}$ or WT HIV_{JRSCF}
532 following either co-culture with an HIV-Gag-specific CTL clone or a parallel No CTL condition. In
533 this assay, puromycin incorporation is used as a readout for metabolic activity in cells. Cells were
534 separated into untreated and oligomycin A treated groups to measure total and glucose
535 dependent metabolism respectively **(A)**, and 2-deoxyglucose treated and dual inhibitor treated
536 groups to measure OXPHOS dependent metabolic activity and shut down both of these arms of
537 metabolism respectively **(B). (C)** Quantification of intracellular ROS accumulation in the same
538 populations as above using CellROX green or DCFH-DA. **(A)-(C)** Show results from 4 donors with
539 P-values calculated by ANNOVA using Tukey's multiple comparisons test. **(D)** Flow cytometry
540 data showing surface CD71 expression in viable bystander and survivor cells surviving killing
541 assays. **(E)** *HIF1A* transcript expression from previous ECCITE-seq of bystander and survivor
542 cells. **(F)** Intracellular protein expression of HIF1-α in the same groups as **(A)-(C)**. For **(D)** P-
543 value from a paired T-test is shown. For **(E)**, P-values of Wilcoxon test is shown.

544 **Figure 5. Induction of oxidative stress with Deferoxamine (DFO) sensitizes HIV-infected**
545 **cells to CTL-mediated elimination. (A)** Representative and summary (n=5 donors) flow
546 cytometry plots showing intracellular ROS accumulation on $HIV_{JRSCF\ TW10esc}$ or WT HIV_{JRSCF}
547 infected cells following 72 hour treatments with either DFO or vehicle (DMSO). **(B)** Representative
548 and summary (n=5 donors) flow cytometry plots measuring surface CD71 expression on HIV_{JRSCF}
549 $_{TW10esc}$ or WT HIV_{JRSCF} infected cells following 72 hour treatments with either DFO or vehicle. **(C**
550 **and D)** Representative (**C**) and summary (**D**) flow cytometry results depicting impact of DFO
551 treatment on CTL-mediated elimination of infected cells. As in other experiments, cells infected
552 with either WT HIV_{JRCSF} (targets/survivors) or escape mutant $HIV_{JRSCF_TW10esc}$ (bystanders) were
553 labeled with different cell-trace dyes and mixed together. Pooled cells were treated with DFO or

554 DMSO (control) and then cultured with or without Gag-TW10-specific CTL. Shown are
555 percentages of infected cells ($CD4^-$, HIV-Gag^+) following gating on cell-trace dyes. **(D)**
556 Quantification of infected-cell killing as ratios of total viable cell counts from plus CTL conditions
557 over no CTL conditions. **(E)** Schematic of proposed mechanisms of ROS-induced cell death
558 mediated by CTL attack and improved by DFO treatment. For **(A), (B)** and **(D)** P-values from
559 paired T-tests are shown.

560 **Figure 6. Molecular features of CTL-resistant infected cells are recapitulated in *ex vivo***
561 **reservoirs from PLWH. (A)-(B)** Re-analysis of memory $CD4^+$ T-cells from PLWH in the antigen-
562 stimulated data set from Collora *et al*., 2022[22] showing unsupervised gene expression clustering
563 of cells and labeling based on HIV RNA expression among T-cell clones. **(C)** Module scoring of
564 metabolism and oxidative stress gene sets enriched in CTL-resistant survivors on the same cells
565 from **(A)-(B)**. **(D)-(E)** UMAP feature plot and violin plots showing gene expression of *BCL2* and
566 surface protein expression of CD155 PVR in bystander and survivor cells. **(F)** Module scoring of
567 CTL-resistant WNN cluster 9 overexpressed genes on HIV RNA- and HIV RNA^+ T.-cell clones
568 from **(A)-(B)**. **(E)** Module scoring of "CD8 cytotoxic" gene set from Szabo *et al*., 2019[36] on HIV
569 RNA- and HIV RNA^+ T-cell clones. All P-values shown are from a Wilcoxon test.

570

571

572 **Supplemental information**

573 Table S1. Related to figure 1G-1F.

574 Table S2. Related to figure 3A.

575 Table S3. Related to figure 6F.

576

577

578

579

580 **SUPPLEMENTARY FIGURE LEGENDS**

581 **Supplementary Figure 1**: **(A)** Schematic of the HIV Infection Model in primary central memory
582 $CD4^+$ T cells. **(B)** Single nucleotide mutation in TW10 epitope of JRCSF converting threonine (T)
583 to asparagine (N) to prevent binding of TW10 antigen to MHC-I. **(C)** Phenotype of HIV infection
584 model by flow cytometry looking at CD45RA, MHC-I and HIV-Gag$^+$ from naïve $CD4^+$ T cells at
585 day 0 to infected $CD4^+$ T_{CM} at day 13 post activation. **(D)** Cytokine staining comparing levels of
586 IFN-γ, IL-17, IL-22 and IL-4 expression on *ex vivo* infected memory $CD4^+$ T cells and non-
587 polarized *in vitro* infection model T_{CM} at day 13 post activation. (**E)** TW10-specific CTL lamp-1
588 (CD107a) degranulation by flow cytometry on 2 donors after a 16h CTL challenge on uninfected
589 cells (grey), $HIV_{JRSCF\ TW10esc}$ -infected cells (blue) and HIV_{JRCSF}-infected cells (red). (**F-G**) Sorting
590 schematic to isolate $HIV_{JRSCF_TW10esc}$ -infected and HIV_{JRCSF}-infected infected cells after coculture
591 (**F**) and without coculture (**G**) with TW10-specific CTL.

592 **Supplementary Figure 2**: **(A)** Abundance of recurring clonotypes from ECCITE-seq data of
593 isolate $HIV_{JRSCF_TW10esc}$ -infected and HIV_{JRCSF}-infected infected cells with no CTL added, or as
594 bystanders and survivors after a CTL killing assay from 1 donor. **(B)** Frequencies of mitochondrial
595 genes in WNN clusters from infected survivor and bystander cell from all 4 donors. **(C)-(H)** Module
596 scores of T-cell activation and functional state gene-sets from Szabo *et al*., 2019[36] on bystander
597 and survivor infected cells from all 4 donors.

598 **Supplementary Figure 3**: **(A)-(D)** Module scores of Hallmark OXPHOS, cholesterol
599 homeostasis, fatty acid metabolism and hypoxia gene-sets on bystander and survivor infected
600 cells from all 4 donors. P-values from Wilcoxon tests are sown.

601 **Supplementary Figure 4**: **(A)-(B)** Representative flow cytometry plots showing viability (top) and
602 CD71 expression (bottom) on bulk $CD4^+$ T-cells after treatment with vehicle and different
603 concentrations of DFO after 24 **(A)** or 72 **(B)** hours of treatment. **(C)** Representative and summary
604 flow cytometry plots showing frequency of HIV-Gag expression in infected $CD4^+$ T-cells treated
605 with vehicle or 10 μM DFO for 72 hours across 5 donors.

606 **Supplementary Figure 5**: **(A)-(B)** Violin plots showing expression of *BCL2* transcript and CD155
607 (PVR) surface protein expression on infected bystander and survivor cells across WNN clusters.
608 **(C)** UMAP feature plot (left) and violin plot (right) showing surface protein expression of MHC-I
609 (HLA-A-B-C) on infected bystander and survivor cells. **(D)** Violin plots showing surface protein
610 expression of MHC-I on infected bystander and survivor cells across WNN clusters. **(E)** Ridge
611 plots showing lower (MHC-I low), middle (MHC-I medium), and upper (MHC-I high) tercile surface
612 protein expression of MHC-I across bystander and survivor cells. **(F)** UMAP projections showing
613 cells clustered by WNN analysis and colored by bystander or survivor cell identity across MHC
614 low, medium and high groups.
615
616 **STAR Methods**
617
618 **KEY RESOURCES TABLE**

REAGENT or RESOURCE	SOURCE	IDENTIFIER
Antibodies		
CD4 BV785 clone OKT4	Biolegend	Cat. #317442
CD4 AF700 clone OKT4	Biolegend	Cat. #317426
CD3 BV785 clone OKT3	Biolegend	Cat. #317330
CD8 BV605 clone SK1	Biolegend	Cat. #344742
CD107a APC/Cyanine 7 clone H4A3	Biolegend	Cat. #328630
CD107a PE clone H4A3	Biolegend	Cat. #328608
CD69 BV650 clone FN50	Biolegend	Cat. # 310934
CD71 Pe/Cyanine 7 clone CY1G4	Biolegend	Cat. # 334112
HLA-A,B,C PE clone W6/32	Biolegend	Cat. # 311406
IL-17 BV605 clone TC11-18H10.1	Biolegend	Cat. # 512325
IL-4 PE/Dazzle™ 594 clone MP4-25D2	Biolegend	Cat. # 500831
IFN-γ Pe/Cyanine 7 clone B27	Biolegend	Cat. # 506518
IL-22 PerCP/Cyanine5.5 clone 2G12A41	Biolegend	Cat. # 366709
TotalSeq-C Human Universal Cocktail V1.0	Biolegend	Cat. # 399905
TotalSeq™-C0251 anti-human Hashtag 1 clones LNH-94; 2M2	Biolegend	Cat. # 394661
TotalSeq™-C0251 anti-human Hashtag 3 clones LNH-94; 2M2	Biolegend	Cat. # 394605
TotalSeq™-C0251 anti-human Hashtag 4 clones LNH-94; 2M2	Biolegend	Cat. # 394607
HIF1- α AF488 clone H1alpha67	Novus Biologicals	Cat. # NB100-105F
Zenon Human IgG labeling Kit AF647	ThermoFisher	Cat. #Z25408

Zenon Human IgG labeling Kit R-PE	ThermoFisher	Cat. #Z25455
N6/PGDM1400x10E8	BEI resources	ARP-13390
PGT121	BEI resources	ARP-12343
Ultra-LEAF™ Purified anti-human CD3 Antibody	Biolegend	Cat. #317325
Ultra-LEAFTM Purified anti-human CD28 Antibody	Biolegend	Cat. #302933
Bacterial and virus strains		
JRCSF	BEI resources	ARP-394
JRCSF TW10escape T242N mutant	Genescript	U1998GG250
JRCSF SL9escape mutant	Genescript	U423KGJ130
Biological samples		
Human peripheral blood leukopak fresh HLA A02 B57	Stemcell	Cat. #70500
Human blood buffy coat	the Gulf Coast Regional Blood Center	
Chemicals, peptides, and recombinant proteins		
TECIN (Teceleukin) Recombinant Human IL2 (rIL-2)	NCI	C166111-01
Recombinant Human IL-15	NCI	NSC. #745101
Dynabeads™ Human T-Activator CD3/CD28 for T Cell Expansion and Activation	ThermoFisher	Cat. #11131D
Anti-Human IL-12	Peprotech	Peprotech 500-P154G
Anti-Human IL-4	Peprotech	Peprotech 500-P24
Recombinant Human TGF-β1	Peprotech	Peprotech 100-21
Cell trace far red (CTFR)	ThermoFisher	Cat. #C34564
Cell trace CFSE	ThermoFisher	Cat. #C34570
Cell trace Violet (CTV)	ThermoFisher	Cat. #C34557
Cell trace Blue (CTB)	ThermoFisher	Cat. #C34574
Live/Dead Fixable Aqua dead cell stain kit	ThermoFisher	Cat. #L34957
Critical commercial assays		
EasySep™ Human Naïve $CD4^+$ T Cell Isolation Kit	Stemcell	Cat. #19555
EasySep Human CD4 Positive Selection Kit II	Stemcell	Cat. #17852
EasySep Human CD8 Positive Selection Kit II	Stemcell	Cat. #17853
Deposited data		
GEO accession number pending		
Experimental models: Cell lines		
HEK 293T Cells	ATCC	

Software and algorithms		
R version 4.3.2	R Core Team (2024)	
FlowJo version 10.10.0	BD Biosciences	

619
620

621 **METHOD DETAILS**

622 **Participants and study approval**

623 Study participants living with HIV were recruited from Whitman Walker Health (Washington, D.C).
624 Leukapheresis samples from deidentified HIV negative individuals were obtained from Stemcell
625 Technologies. Ethical approval to conduct this study was obtained from George Washington
626 University and the Weill Cornell Medicine Institutional Review Boards (Weill Cornel Medicine
627 #1805019252 and George Washington University FWA#00005945). All participants were adults
628 and provided written informed consent.

629 **HIV infection model in cultured central memory CD4$^+$ T cells (T_{CM}):**

630 The infection model was adapted from a previously described HIV latency model[30,31]. Peripheral
631 blood mononuclear cells (PBMCs) were isolated from leukapheresis samples from HIV negative
632 donors obtained from Stemcell technologies. Naïve CD4$^+$ T cells were magnetically isolated from
633 thawed PBMCs using the EasySep™ Human Naïve CD4$^+$ T Cell Isolation Kit (Stemcell) according
634 to the manufacturer's instructions. Purified naïve CD4$^+$ T cells were then activated using human
635 anti-CD3/CD28-coated magnetic beads (one bead for two cells, Gibco Cat. #11131D) in the
636 presence of human anti-IL-4 (1µg/10^6 cells Peprotech 500-P24), human anti-IL-12 (2µg/10^6 cells
637 Peprotech 500-P154G), and Tumor Growth Factor (TGF)-β1 (10ng/10^6 Peprotech 100-21) to
638 prevent cell polarization. After 3 days, cells were maintained at a concentration of 10^6 cells /mL
639 in media containing 50 IU of human recombinant IL-2. At day 7, the cultured T_{CM} were infected
640 with either WT HIV_{JRCSF} or $HIV_{JRCSF\ TW10escape}$. One quarter of the cells were infected by the addition

641 of 200 units of virus (see virus production details below for unit description) per $1x10^7$ cells in 1mL
642 and centrifugation at 1500xg for 2h at 37°C. Following this 'spinoculation', the infected cell cultures
643 were mixed in flasks containing the remaining three quarters of the cells at $2x10^6$ cells/mL in media
644 containing 50 IU of human recombinant IL-2. At day 10, the cells were crowded in 96-well round
645 bottom plates at a density of $2x10^5$ cells/200uL/well to enhance cell-to-cell transmission of HIV.
646 On day 13, cells were cryopreserved in FBS with 10% DMSO and stored in liquid nitrogen for
647 future experiments.

648 **Virus production and infections:**

649 JRCSF WT and JRCSF TW10esc plasmids were obtained from BEI-resources and Genscript,
650 respectively. Plasmids were expanded using Stlb3 competent cells and maxi-prep from Qiagen
651 (QIAGEN Plasmid Maxi Kit (25)). Plasmids were transfected into HEK 293T cells using Optimem
652 media and FuGENE® 6 Transfection Reagent (Promega). Media was exchanged 24h after
653 transfection for DMEM with 10% FBS. Two days following the media change, supernatants were
654 passed through 0.45μm filters. Viruses were then concentrated overnight at 4°C using the PEG-
655 it virus precipitation solution (System Biosciences) following the manufacturer's instructions.
656 Finally, the concentrated virus was frozen in aliquots of 200 µl. Across multiple titration
657 experiments, 200 µl of virus for 1 x 10^7 cells gave the most optimal results balancing infection
658 efficiency and viability of productively infected cells.

659 **Isolation and expansion of HIV specific Cytotoxic T- lymphocytes (CTLs):**

660 CTL specific for HIV epitopes Gag-TW10 and Gag-SL9 were isolated from PBMCs of 3 donors
661 living with HIV. Briefly, 10 x 10^6 PBMCs were peptide pulsed with HIV optimal peptides TW10
662 (TSTLQEQIGW, Gag residues 240-249) or SL9 (SLYNTVATL Gag residues 77-85) at 1μg/mL for
663 16h at 37°C in XVIVO-15 media. T cells that responded to the peptide by secreting IFN-γ were
664 isolated using an IFN-γ secretion assay – Cell Enrichment and Detection Kit (PE) (Miltenyi
665 Cat#130-054-202). The cells were then serially diluted and stimulated with PBMCs from HIV-

666 negative donors that had been irradiated with 5,000 Rad, along with soluble anti-CD3/anti-CD28
667 in media containing 50IU IL-2 and 0.51ng/mL IL-15. Wells for selected from dilutions in which <1/5
668 wells showed growth, giving confidence that the cells in each well were derived from a single
669 clone. CTL specificities were assessed by flow cytometry by assessing degranulation (CD107a
670 surface exposure) upon the addition of 1μg/mL of the respective peptide.

671 **Killing assays and sequential killing assays:**

672 Infected cells from the previously described HIV Infection Model in cultured T_{CM} were thawed and
673 rested for 2 days at 2 x 10^6 cells per mL in media containing 50 IU of human IL-2. Prior to co-
674 culture with CTL, cells expressing high levels of CD4 were depleted by magnetic selection using
675 the EasySep™ Human CD4 Positive Selection Kit II (Stemcell); this step enriches for $CD4^-$
676 infected cells (since HIV-infected cells downregulate CD4). Cells infected with WT HIV_{JRCSF} were
677 labeled with cell trace far red (CTFR) (dilution 1:20,000) and cells infected with $HIV_{JRCSF\ TW10escape}$
678 were labeled with cell trace carboxyfluorescein succinimidyl ester (CFSE) (dilution 1:5,000).
679 CTFR-labeled WT HIV_{JRCSF}-infected cells were mixed with CFSE-labeled $HIV_{JRCSF\ TW10escape}$-
680 infected cells at a ratio of 2:1 and 6 x 10^5 cells from these mixed populations were aliquoted into
681 wells of a 96-well plate. 3 x 10^5 CTL clones specific for the HIV-Gag epitope TW10
682 'TSTLQEQIGW' were labeled with CellTrace™ Violet (CTV) (dilution 1:10,000) and were added
683 to each well at a 1:2 effector:target ratio along with anti-CD107a APC-Cy7 (dilution 1:200). Killing
684 assays were performed in R10 (RPMI 1640 supplemented with 10% FBS and 1%
685 penicillin/streptomycin, 1% HEPES buffer, 5 mM L-Glutamine), with 50 IU of human recombinant
686 IL-2 and 0.51 ng/mL of human recombinant IL-15 for 16h at 37°C. For Sequential Killing Assays,
687 CTL were then removed by magnetic selection using the EasySep™ Human CD8 Positive
688 Selection Kit II (Stemcell) and a fresh batch of CTL clone specific for the HIV-Gag epitope SL9
689 'SLYNTVATL' were added for the second round of killing, which was again for 16h at 37°C (no
690 CTL control conditions were maintained in parallel). Post-second killing assay, the levels of

691 infected cells were assessed by flow cytometry, staining extracellularly with anti-CD3 (OKT3,
692 Biolegend), anti-CD4 (OKT4, Biolegend), anti-CD8 (SK1, Biolegend) antibodies and Live/Dead
693 fixable Aqua stain (Thermofisher). Cells were then fixed with the BD Cytofix/Cytoperm™
694 Fixation/Permeabilization Kit according to the manufacturer's instructions and intracellularly
695 stained using an anti-HIV-Gag antibody (KC57, Beckman Coulter) before analysis on an Attune
696 NxT flow cytometer.

697 **Sorting for 'survivors' and 'bystanders' following killing assays:**

698 Killing assays were set up as described above, with minor differences. For these sorting assays,
699 cells infected with WT HIV_{JRCSF} were labeled with CFSE (dilution 1:5,000) and cells infected with
700 $HIV_{JRCSF\ TW10escape}$ were labeled with CTV (dilution 1:10,000). These were then mixed together
701 before adding a TW10-specific CTL that had been labeled with CellTrace™ Blue CTB (dilution
702 1:10,000). No CTL control conditions were cultured in parallel. Post-killing, cells were harvested
703 for staining with anti-CD4 BV785 (1:100), Live/Dead fixable Aqua (1:200), bNAbs PGT121
704 conjugated with Zenon Kit PE (1µg per 1 x 10^6 cells) and bNAbs N6/PGDM1400x10E8 conjugated
705 with Zenon Kit AF647 (1µg per 1 x 10^6 cells) at 37°C for 1h. Live cells productively infected CFSE-
706 labeled WT HIV_{JRCSF} and CTV-labeled $HIV_{JRCSF\ TW10escape}$ were sorted by gating on the double
707 positive population for PGT121 and N6/PGDM1400x10E8.

708 **Flow cytometry for SCENITH metabolic profiling:**

709 Infected bystander and target/survivor cells after a 'killing assay' with or without the addition of
710 CTL were treated in R10 media as previously described[44], with a few modifications. Briefly, cells
711 were treated for 60 minutes with DMSO or with the following metabolic inhibitors - 2-Deoxy-D-
712 Glucose (DG, final concentration 100mM), Oligomycin (Oligo, final concentration 1µM), or a
713 combination of the drugs at the same final concentrations. Puromycin (final concentration
714 10µg/ml) was added during the last 30 minutes of the treatments with the metabolic inhibitors.
715 Single-cell suspensions were stained for surface markers using the following antibodies anti-CD4
716 (OKT4, Biolegend), anti-CD8 (SK1, Biolegend), anti-CD7 (CD7-6B7, Biolegend), anti-CD71

717 (CY1G4, biolegend), anti-CD69 (FN50, Biolegend), anti-CD45RA (HI100, Biolegend) and anti-
718 HLA-A-B-C (W6/32, Biolegend) along with a fixable live/dead stain (Thermofisher), in PBS for 30
719 minutes at 37°C. Cells were washed and fixed with 1X eBioscience™ FoxP3/transcription factor
720 fixation/permeabilization solution (Thermofisher) for 45 minutes at 4°C. This fixation solution was
721 washed away and cells were stained intracellularly with anti-HIV-Gag-p24 (KC57, Beckman
722 Coulter), anti-puromycin (2A4, Biolegend) and HIF1-α (H1alpha67, Novus Biologicals) antibodies
723 in 1X FoxP3/transcription factor permeabilization solution (Thermofisher) for 60 minutes at 37°C.
724 Cells were washed one more time before analysis on an Attune NxT flow cytometry instrument.

725 **Flow cytometry for ROS accumulation:**

726 Infected bystander and target cells after a 'killing assay', with or without the addition of CTL, were
727 treated with 500 nM CellROX green (Thermofisher) or 0.2X DCFH-DA (CELL BIOLABS) for 1
728 hour. CellROX solution was washed and single cell suspensions were stained using surface target
729 antibodies against CD4 (OKT4, Biolegend), CD8 (SK1, Biolegend), CD7 (CD7-6B7, Biolegend),
730 CD71 (CY1G4, biolegend), CD69 (FN50, Biolegend), CD45RA (HI100, Biolegend) and HLA-A-B-
731 C (W6/32, Biolegend) along with a fixable live/dead stain (Thermofisher) in PBS for 30 minutes at
732 37°C. Cells were washed and then fixed with 1X Cytofix/Cytoperm™ solution (BD) for 20 minutes
733 at room temperature. Fixation solutions were washed away and cells were stained intracellularly
734 with anti-HIV-Gag-p24 (KC57, Beckman Coulter) antibody in 1X Perm/Wash™ (BD) for 30
735 minutes at 37°C. Cells were washed one more time before analysis on an Attune NxT flow
736 cytometry instrument.

737 **ECCITE-seq compatible with a 10X genomics instrument:**

738 Cells were stained with DNA oligo-barcoded antibodies and loaded onto the 10x Chromium
739 single-cell workflow (10X Genomics) as previously described[34] with a few modifications.
740 Approximately 0.05-0.3 x 10^6 cells per sample were resuspended in R10 media and incubated
741 with the TotalSeq™-C Human Universal Cocktail (Biolegend) for 30 minutes at 4°C. In some

742 cases, TotalSeq™-C hashing antibodies #1, #3 and #4 (Biolegend) were spiked into individual
743 samples, which allowed for multiplexing of survivor, bystanders and cells with no CTL into the
744 same 10X lane. After staining, cells were washed 3 times in R10 media, followed by centrifugation
745 (400 × g for 5 minutes at 4°C) and supernatant aspiration. After the final wash, cells were
746 resuspended in PBS and filtered through 70-µm cell strainers. Stained cells from each sample
747 were pooled and loaded into the 10x Chromium Single Cell Immune Profiling workflow
748 (CG000330, revision G). Libraries were generated according to the 10x Chromium Single Cell
749 Immune Profiling workflow instructions, pooled and sequenced on Illumina NovaSeq 6000 or a
750 NovaSeq X.

751 **Single-cell data alignment:**

752 FASTQ files from the 10x gene expression, surface protein and TCR α/β libraries were processed
753 using Cell Ranger v7.0.1 (10x Genomics), using either the count or the multi pipeline (when TCR
754 libraries were available) with default parameters.

755 RNA transcripts from ECCITE-seq were mapped to a modified version of Cell Ranger's GRCh38-
756 2020-A reference package (GRCh38 / GENCODE v32 annotations), with the addition of the HIV-
757 1 HXB2 reference sequence. TCR α/β libraries were mapped to Cell Ranger's cellranger-vdj-
758 GRCh38-alts-ensembl-7.1.0 reference package.

759 **Initial cell/gene level filtering:**

760 For cell filtering, cell barcodes with <200, >8,000 genes expressed or > 10% mitochondrial genes
761 expressed were removed. For gene-level filtering, genes were filtered such that only those
762 expressed at a level of <200 UMI or in < 3 cells were removed.

763 These cell- and gene-level filtered gene/barcode matrices were used for downstream analysis.

764 **Seurat normalization:**

765 The count matrices of all modalities were loaded into a Seurat v5 object (Seurat version 5.1.0).
766 For gene expression (GEX) data, we normalized the count data using LogNormalize and scaled
767 the resulting normalized values using ScaleData. For all other modalities (ADT, HTO, TCR α/β),

768 we normalized the count data using centered-log ratio (margin = 2) and scaled the resulting
769 normalized values using ScaleData.

770 **Hashing antibody demultiplexing:**

771 To separate individual samples from pooled cell libraries, samples were demultiplexed by their
772 HTO using Seurat HTODemux with the positive quantile parameter set to 0.999.

773 **Harmony integration of GEX and ADT modalities across donors:**

774 To integrate datasets from different donors across separate 10X runs, datasets from each donor
775 were first merged into one object using the merge Seurat function and then we used RunHarmony
776 as previously described on GEC and ADT modalities to remove dataset-of-origin cell embeddings
777 using the "batch" covariate, in this case "donor" included in the objects metadata[68]. Cells were
778 then given probabilistic cluster membership based on K-means cluster centroids localization for
779 each modality.

780 **Multimodal WNN analysis:**

781 We applied weighted-nearest neighbor (WNN) analysis on our ECCITE-seq data, enabling the
782 integrative analysis of GEX and ADT modalities in the same cells as previously described[20].
783 Briefly, k-nearest neighbors graphs (k = 20) were first constructed, and the neighbors of each cell
784 in each modality were identified using FindMultiModalNeighbors in Seurat V5. For graph
785 construction, the first 15 principal components (PCs) of the log-normalized values from the GEX
786 modality and the first 12 PCs of the centered-log ratio values from the ADT modality were used.
787 The dimensionally reduced molecular profiles of the k-nearest neighbors of each cell were then
788 averaged and compared with the actual values to obtain the residuals in an RNA-RNA, protein-
789 protein and RNA-protein manner. Residuals were converted into affinity-based similarities using
790 UMAP. Ratios of the within-modality and cross-modality affinities were softmax transformed to
791 obtain the cell-specific modality weights. The weighted similarity then formed the basis of the
792 construction of the WNN graph visualized on a WNN integrated UMAP. Clusters were called using
793 the FindClusters function at a resolution of 0.5.

794 **Additional cell filters:**

795 WNN clusters 3 and 10 were filtered out after initial analysis due to disproportionately high
796 expression of MT-genes compared to other clusters. Cells having > 0 normalized expression of
797 *CD8A or CD8B* transcripts or > 0.5 normalized expression of CD8 protein were filtered out from
798 further analysis.

799 **Differential gene expression and pathway enrichment analysis:**

800 Differential gene expression analysis across WNN clusters was performed using FindAllMarkers.
801 The logfc.threshold (minimum log_2 fold change) was set to 0.25 and min.pct (minimum proportion
802 of cells expressing the given gene) was set to 0.25 to avoid inclusion of poorly expressed genes
803 that can skew differential gene expression results. Only genes with an adjusted P-value of < 0.05
804 were further considered. Row normalized Z-scores from using scale.data were used for
805 visualization on the heatmap focusing on the top 10 differentially expressed genes.

806 Genes passing the above filters were used for pathway enrichment analysis. ClusterProfiler was
807 used to profile gene clusters on Gene Ontology terms. Specifically the biological process (GO:BP)
808 subontology was used for enrichment analysis. Gene ontology terms were considered significant
809 if the FDR-adjusted P values was < 0.05.

810 Similarly, total bystander and survivor populations were compared using FindAllMarkers with the
811 logfc.threshold set to 0.1 and min.pct set to 0.1. Top 30 differentially expressed genes were used
812 for visualization on the heatmap showing row-normalized Z-scores. Genes passing the
813 logfc.threshold and min.pct filters were used for pathway enrichment analysis with ClusterProfiler
814 as above but using both the GO:BP subontology as well as Reactome for gene cluster profiling
815 and visualization.

816 **Module scoring on bystander and survivor cells from T_{CM}-infection model:**

817 The AddModuleScore function of Seurat V5 was used for scoring gene expression modules. For
818 Hallmark and Gene Ontology gene-sets, the msigdbr package was used to pull selected gene-
819 sets from the Molecular Signatures Database (MSigDB).

820 T-cell activation and functionality gene-sets were pulled from Szabo *et* al., 2019[36]. The cytotoxic
821 WNN cluster 9 gene-set was constructed from the results of differential gene expression analysis
822 comparing WNN cluster 9 to all other clusters after all unwanted cell removal filter steps using the
823 FindMarkers function and setting min.pct = 0.1 and logfc.threshold = 0.05. Genes were then
824 filtered for those significantly overexpressed by WNN cluster 9 subletting on those with $\log_2$ fold
825 change > 0.05 and adjusted P-value < 0.05.

826 **Module scoring on HIV RNA$^+$ and HIV RNA- T-cell clones from PLWH:**

827 Single cell transcriptional and V(D)J reconstruction data from *ex vivo* antigen stimulated CD4$^+$ T-
828 cell clones from PLWH was pulled from Collora *et al*., 2022[22]. HIV RNA$^+$ T cell clone cells were
829 defined as 2 or more cells expressing the same CDR3 having at least one HIV-1 RNA$^+$ cell. HIV
830 RNA- T-cell clones were defined as 2 or more cells expressing the same CDR3 with no member
831 expressing HIV transcripts. As above, the AddModuleScore function of Seurat V5 was used for
832 scoring gene expression modules of Hallmark and Gene On The AddModuleScore function of
833 Seurat V5 was used for scoring gene expression modules of Hallmark and Gene Ontology gene-
834 sets from MSigDB using msigdbr, the "CD8 cytotoxic" functional state from Szabo *et* al., 2019[36],
835 and the WNN cluster 9 overexpressed gene-set

836

837 **RESOURCE AVAILABILITY**

838 **Data and code availability**

839 ECCITE-seq data is being deposited to GEO. The accession number will be listed in the key
840 resources table. This paper does not report original code.

841

842

843

844

845

References

1. Chun, T.W., Stuyver, L., Mizell, S.B., Ehler, L.A., Mican, J.A., Baseler, M., Lloyd, A.L., Nowak, M.A., and Fauci, A.S. (1997). Presence of an inducible HIV-1 latent reservoir during highly active antiretroviral therapy. Proc Natl Acad Sci U S A *94*, 13193-13197. 10.1073/pnas.94.24.13193.
2. Wong, J.K., Hezareh, M., Gunthard, H.F., Havlir, D.V., Ignacio, C.C., Spina, C.A., and Richman, D.D. (1997). Recovery of replication-competent HIV despite prolonged suppression of plasma viremia. Science *278*, 1291-1295. 10.1126/science.278.5341.1291.
3. Finzi, D., Hermankova, M., Pierson, T., Carruth, L.M., Buck, C., Chaisson, R.E., Quinn, T.C., Chadwick, K., Margolick, J., Brookmeyer, R., et al. (1997). Identification of a reservoir for HIV-1 in patients on highly active antiretroviral therapy. Science *278*, 1295-1300. 10.1126/science.278.5341.1295.
4. Lee, G.Q., Orlova-Fink, N., Einkauf, K., Chowdhury, F.Z., Sun, X., Harrington, S., Kuo, H.H., Hua, S., Chen, H.R., Ouyang, Z., et al. (2017). Clonal expansion of genome-intact HIV-1 in functionally polarized Th1 CD4+ T cells. J Clin Invest *127*, 2689-2696. 10.1172/JCI93289.
5. Bui, J.K., Sobolewski, M.D., Keele, B.F., Spindler, J., Musick, A., Wiegand, A., Luke, B.T., Shao, W., Hughes, S.H., Coffin, J.M., et al. (2017). Proviruses with identical sequences comprise a large fraction of the replication-competent HIV reservoir. PLoS Pathog *13*, e1006283. 10.1371/journal.ppat.1006283.
6. Cohn, L.B., Silva, I.T., Oliveira, T.Y., Rosales, R.A., Parrish, E.H., Learn, G.H., Hahn, B.H., Czartoski, J.L., McElrath, M.J., Lehmann, C., et al. (2015). HIV-1 integration landscape during latent and active infection. Cell *160*, 420-432. 10.1016/j.cell.2015.01.020.
7. Huang, S.-H., Ren, Y., Thomas, A.S., Chan, D., Mueller, S., Ward, A.R., Patel, S., Bollard, C.M., Cruz, C.R., Karandish, S., et al. (2018). Latent HIV reservoirs exhibit inherent resistance to elimination by CD8+ T cells. The Journal of Clinical Investigation *128*, 876-889. 10.1172/JCI97555.
8. Ren, Y., Huang, S.H., Patel, S., Alberto, W.D.C., Magat, D., Ahimovic, D., Macedo, A.B., Durga, R., Chan, D., Zale, E., et al. (2020). BCL-2 antagonism sensitizes cytotoxic T cell–resistant HIV reservoirs to elimination ex vivo. The Journal of Clinical Investigation *130*, 2542-2559. 10.1172/JCI132374.
9. Leyre, L., Kroon, E., Vandergeeten, C., Sacdalan, C., Colby, D.J., Buranapraditkun, S., Schuetz, A., Chomchey, N., de Souza, M., Bakeman, W., et al. (2020). Abundant HIV-infected cells in blood and tissues are rapidly cleared upon ART initiation during acute HIV infection. Sci Transl Med *12*. 10.1126/scitranslmed.aav3491.
10. Lian, X., Seiger, K.W., Parsons, E.M., Gao, C., Sun, W., Gladkov, G.T., Roseto, I.C., Einkauf, K.B., Osborn, M.R., Chevalier, J.M., et al. (2023). Progressive transformation of the HIV-1 reservoir cell profile over two decades of antiviral therapy. Cell Host Microbe *31*, 83-96 e85. 10.1016/j.chom.2022.12.002.
11. Sun, W., Gao, C., Gladkov, G.T., Roseto, I., Carrere, L., Parsons, E.M., Gasca-Capote, C., Frater, J., Fidler, S., Yu, X.G., et al. (2024). Footprints of innate immune activity during HIV-1 reservoir cell evolution in early-treated infection. J Exp Med *221*. 10.1084/jem.20241091.
12. Sun, W., Gao, C., Hartana, C.A., Osborn, M.R., Einkauf, K.B., Lian, X., Bone, B., Bonheur, N., Chun, T.W., Rosenberg, E.S., et al. (2023). Phenotypic signatures of immune selection in HIV-1 reservoir cells. Nature *614*, 309-317. 10.1038/s41586-022-05538-8.

895 13. Chun, T.W., Finzi, D., Margolick, J., Chadwick, K., Schwartz, D., and Siliciano, R.F.
896 (1995). In vivo fate of HIV-1-infected T cells: quantitative analysis of the transition to
897 stable latency. Nat Med *1*, 1284-1290. 10.1038/nm1295-1284.
898 14. Jiang, C., Lian, X., Gao, C., Sun, X., Einkauf, K.B., Chevalier, J.M., Chen, S.M.Y., Hua,
899 S., Rhee, B., Chang, K., et al. (2020). Distinct viral reservoirs in individuals with
900 spontaneous control of HIV-1. Nature *585*, 261-267. 10.1038/s41586-020-2651-8.
901 15. Richter E, B.T., Büning A, Korencak M, Crowell T.A, Jessen H, Rockstroh J.K, Esser S,
902 Boesecke C, Streeck H. (2024). Ultra-low level HIV p24 production as a Driver of
903 Immune Activation in Individuals Treated with ART. CROI.
904 16. Einkauf, K.B., Osborn, M.R., Gao, C., Sun, W., Sun, X., Lian, X., Parsons, E.M.,
905 Gladkov, G.T., Seiger, K.W., Blackmer, J.E., et al. (2022). Parallel analysis of
906 transcription, integration, and sequence of single HIV-1 proviruses. Cell *185*, 266-282
907 e215. 10.1016/j.cell.2021.12.011.
908 17. Thomas, A.S., Jones, K.L., Gandhi, R.T., McMahon, D.K., Cyktor, J.C., Chan, D.,
909 Huang, S.H., Truong, R., Bosque, A., Macedo, A.B., et al. (2017). T-cell responses
910 targeting HIV Nef uniquely correlate with infected cell frequencies after long-term
911 antiretroviral therapy. PLoS Pathog *13*, e1006629. 10.1371/journal.ppat.1006629.
912 18. Stevenson, E.M., Ward, A.R., Truong, R., Thomas, A.S., Huang, S.H., Dilling, T.R.,
913 Terry, S., Bui, J.K., Mota, T.M., Danesh, A., et al. (2021). HIV-specific T cell responses
914 reflect substantive in vivo interactions with antigen despite long-term therapy. JCI Insight
915 *6*. 10.1172/jci.insight.142640.
916 19. Stevenson, E.M., Terry, S., Copertino, D., Leyre, L., Danesh, A., Weiler, J., Ward, A.R.,
917 Khadka, P., McNeil, E., Bernard, K., et al. (2022). SARS CoV-2 mRNA vaccination
918 exposes latent HIV to Nef-specific CD8(+) T-cells. Nat Commun *13*, 4888.
919 10.1038/s41467-022-32376-z.
920 20. Dube, M., Tastet, O., Dufour, C., Sannier, G., Brassard, N., Delgado, G.G., Pagliuzza,
921 A., Richard, C., Nayrac, M., Routy, J.P., et al. (2023). Spontaneous HIV expression
922 during suppressive ART is associated with the magnitude and function of HIV-specific
923 CD4(+) and CD8(+) T cells. Cell Host Microbe *31*, 1507-1522 e1505.
924 10.1016/j.chom.2023.08.006.
925 21. Takata, H., Mitchell, J.L., Pacheco, J., Pagliuzza, A., Pinyakorn, S., Buranapraditkun, S.,
926 Sacdalan, C., Leyre, L., Nathanson, S., Kakazu, J.C., et al. (2023). An active HIV
927 reservoir during ART is associated with maintenance of HIV-specific CD8(+) T cell
928 magnitude and short-lived differentiation status. Cell Host Microbe *31*, 1494-1506 e1494.
929 10.1016/j.chom.2023.08.012.
930 22. Collora, J.A., Liu, R., Pinto-Santini, D., Ravindra, N., Ganoza, C., Lama, J.R., Alfaro, R.,
931 Chiarella, J., Spudich, S., Mounzer, K., et al. (2022). Single-cell multiomics reveals
932 persistence of HIV-1 in expanded cytotoxic T cell clones. Immunity *55*, 1013-1031
933 e1017. 10.1016/j.immuni.2022.03.004.
934 23. Chomont, N., El-Far, M., Ancuta, P., Trautmann, L., Procopio, F.A., Yassine-Diab, B.,
935 Boucher, G., Boulassel, M.R., Ghattas, G., Brenchley, J.M., et al. (2009). HIV reservoir
936 size and persistence are driven by T cell survival and homeostatic proliferation. Nat Med
937 *15*, 893-900. 10.1038/nm.1972.
938 24. Yeh, Y.J., Yang, K., Razmi, A., and Ho, Y.C. (2021). The Clonal Expansion Dynamics of
939 the HIV-1 Reservoir: Mechanisms of Integration Site-Dependent Proliferation and HIV-1
940 Persistence. Viruses *13*. 10.3390/v13091858.
941 25. McKenzie, B., Khazen, R., and Valitutti, S. (2022). Greek Fire, Poison Arrows, and
942 Scorpion Bombs: How Tumor Cells Defend Against the Siege Weapons of Cytotoxic T
943 Lymphocytes. Front Immunol *13*, 894306. 10.3389/fimmu.2022.894306.
944 26. Ren, Y., Huang, S.H., Patel, S., Alberto, W.D.C., Magat, D., Ahimovic, D., Macedo, A.B.,
945 Durga, R., Chan, D., Zale, E., et al. (2020). BCL-2 antagonism sensitizes cytotoxic T

946 cell-resistant HIV reservoirs to elimination ex vivo. J Clin Invest *130*, 2542-2559.
947 10.1172/JCI132374.
948 27. Kishton, R.J., Patel, S.J., Decker, A.E., Vodnala, S.K., Cam, M., Yamamoto, T.N., Patel,
949 Y., Sukumar, M., Yu, Z., Ji, M., et al. (2022). Cancer genes disfavoring T cell immunity
950 identified via integrated systems approach. Cell Rep *40*, 111153.
951 10.1016/j.celrep.2022.111153.
952 28. Joung, J., Kirchgatterer, P.C., Singh, A., Cho, J.H., Nety, S.P., Larson, R.C., Macrae,
953 R.K., Deasy, R., Tseng, Y.Y., Maus, M.V., and Zhang, F. (2022). CRISPR activation
954 screen identifies BCL-2 proteins and B3GNT2 as drivers of cancer resistance to T cell-
955 mediated cytotoxicity. Nat Commun *13*, 1606. 10.1038/s41467-022-29205-8.
956 29. Bory, R., and Caplier, P. (1965). [Gynecology]. Gaz Med Fr *72*, 3709-3716.
957 30. Messi, M., Giacchetto, I., Nagata, K., Lanzavecchia, A., Natoli, G., and Sallusto, F.
958 (2003). Memory and flexibility of cytokine gene expression as separable properties of
959 human T(H)1 and T(H)2 lymphocytes. Nat Immunol *4*, 78-86. 10.1038/ni872.
960 31. Bosque, A., and Planelles, V. (2009). Induction of HIV-1 latency and reactivation in
961 primary memory CD4+ T cells. Blood *113*, 58-65. 10.1182/blood-2008-07-168393.
962 32. Koyanagi, Y., Miles, S., Mitsuyasu, R.T., Merrill, J.E., Vinters, H.V., and Chen, I.S.Y.
963 (1987). Dual Infection of the Central Nervous System by AIDS Viruses with Distinct
964 Cellular Tropisms. Science *236*, 819-822. doi:10.1126/science.3646751.
965 33. Kaplan, D.H., Shankaran, V., Dighe, A.S., Stockert, E., Aguet, M., Old, L.J., and
966 Schreiber, R.D. (1998). Demonstration of an interferon gamma-dependent tumor
967 surveillance system in immunocompetent mice. Proc Natl Acad Sci U S A *95*, 7556-
968 7561. 10.1073/pnas.95.13.7556.
969 34. Herrera, A., Cheng, A., Mimitou, E.P., Seffens, A., George, D., Bar-Natan, M., Heguy,
970 A., Ruggles, K.V., Scher, J.U., Hymes, K., et al. (2021). Multimodal single-cell analysis
971 of cutaneous T-cell lymphoma reveals distinct subclonal tissue-dependent signatures.
972 Blood *138*, 1456-1464. 10.1182/blood.2020009346.
973 35. Mimitou, E.P., Cheng, A., Montalbano, A., Hao, S., Stoeckius, M., Legut, M., Roush, T.,
974 Herrera, A., Papalexi, E., Ouyang, Z., et al. (2019). Multiplexed detection of proteins,
975 transcriptomes, clonotypes and CRISPR perturbations in single cells. Nat Methods *16*,
976 409-412. 10.1038/s41592-019-0392-0.
977 36. Szabo, P.A., Levitin, H.M., Miron, M., Snyder, M.E., Senda, T., Yuan, J., Cheng, Y.L.,
978 Bush, E.C., Dogra, P., Thapa, P., et al. (2019). Single-cell transcriptomics of human T
979 cells reveals tissue and activation signatures in health and disease. Nat Commun *10*,
980 4706. 10.1038/s41467-019-12464-3.
981 37. Locksley, R.M., Killeen, N., and Lenardo, M.J. (2001). The TNF and TNF receptor
982 superfamilies: integrating mammalian biology. Cell *104*, 487-501. 10.1016/s0092-
983 8674(01)00237-9.
984 38. Subramanian Vignesh, K., and Deepe, G.S., Jr. (2017). Metallothioneins: Emerging
985 Modulators in Immunity and Infection. Int J Mol Sci *18*. 10.3390/ijms18102197.
986 39. Yu, M., Li, G., Lee, W.W., Yuan, M., Cui, D., Weyand, C.M., and Goronzy, J.J. (2012).
987 Signal inhibition by the dual-specific phosphatase 4 impairs T cell-dependent B-cell
988 responses with age. Proc Natl Acad Sci U S A *109*, E879-888.
989 10.1073/pnas.1109797109.
990 40. Buck, M.D., O'Sullivan, D., and Pearce, E.L. (2015). T cell metabolism drives immunity. J
991 Exp Med *212*, 1345-1360. 10.1084/jem.20151159.
992 41. Tirosh, I., Izar, B., Prakadan, S.M., Wadsworth, M.H., 2nd, Treacy, D., Trombetta, J.J.,
993 Rotem, A., Rodman, C., Lian, C., Murphy, G., et al. (2016). Dissecting the multicellular
994 ecosystem of metastatic melanoma by single-cell RNA-seq. Science *352*, 189-196.
995 10.1126/science.aad0501.

42. Akkaya, B., Roesler, A.S., Miozzo, P., Theall, B.P., Al Souz, J., Smelkinson, M.G., Kabat, J., Traba, J., Sack, M.N., Brzostowski, J.A., et al. (2018). Increased Mitochondrial Biogenesis and Reactive Oxygen Species Production Accompany Prolonged CD4(+) T Cell Activation. J Immunol *201*, 3294-3306. 10.4049/jimmunol.1800753.
43. Shu, P., Liang, H., Zhang, J., Lin, Y., Chen, W., and Zhang, D. (2023). Reactive oxygen species formation and its effect on CD4(+) T cell-mediated inflammation. Front Immunol *14*, 1199233. 10.3389/fimmu.2023.1199233.
44. Arguello, R.J., Combes, A.J., Char, R., Gigan, J.P., Baaziz, A.I., Bousiquot, E., Camosseto, V., Samad, B., Tsui, J., Yan, P., et al. (2020). SCENITH: A Flow Cytometry-Based Method to Functionally Profile Energy Metabolism with Single-Cell Resolution. Cell Metab *32*, 1063-1075 e1067. 10.1016/j.cmet.2020.11.007.
45. Reiniers, M.J., van Golen, R.F., Bonnet, S., Broekgaarden, M., van Gulik, T.M., Egmond, M.R., and Heger, M. (2017). Preparation and Practical Applications of 2',7'-Dichlorodihydrofluorescein in Redox Assays. Anal Chem *89*, 3853-3857. 10.1021/acs.analchem.7b00043.
46. Bode, K., Link, C., Krammer, P.H., and Weyd, H. (2020). Flow-cytometric Detection of Low-level Reactive Oxygen Species in Cell Lines and Primary Immune Cells. Bio Protoc *10*, e3737. 10.21769/BioProtoc.3737.
47. Tao, J.H., Barbi, J., and Pan, F. (2015). Hypoxia-inducible factors in T lymphocyte differentiation and function. A Review in the Theme: Cellular Responses to Hypoxia. Am J Physiol Cell Physiol *309*, C580-589. 10.1152/ajpcell.00204.2015.
48. Martinvalet, D., Dykxhoorn, D.M., Ferrini, R., and Lieberman, J. (2008). Granzyme A cleaves a mitochondrial complex I protein to initiate caspase-independent cell death. Cell *133*, 681-692. 10.1016/j.cell.2008.03.032.
49. Jacquemin, G., Margiotta, D., Kasahara, A., Bassoy, E.Y., Walch, M., Thiery, J., Lieberman, J., and Martinvalet, D. (2015). Granzyme B-induced mitochondrial ROS are required for apoptosis. Cell Death Differ *22*, 862-874. 10.1038/cdd.2014.180.
50. Kong, Y., Liu, P.K., Li, Y., Nolan, N.D., Quinn, P.M.J., Hsu, C.W., Jenny, L.A., Zhao, J., Cui, X., Chang, Y.J., et al. (2023). HIF2alpha activation and mitochondrial deficit due to iron chelation cause retinal atrophy. EMBO Mol Med *15*, e16525. 10.15252/emmm.202216525.
51. Babcock, J., Herrera, A., Coricor, G., Karch, C., Liu, A.H., Rivera-Gines, A., and Ko, J.L. (2017). Mechanism Governing Human Kappa-Opioid Receptor Expression under Desferrioxamine-Induced Hypoxic Mimic Condition in Neuronal NMB Cells. Int J Mol Sci *18*. 10.3390/ijms18010211.
52. Chen, C., Liu, P., Duan, X., Cheng, M., and Xu, L.X. (2019). Deferoxamine-induced high expression of TfR1 and DMT1 enhanced iron uptake in triple-negative breast cancer cells by activating IL-6/PI3K/AKT pathway. Onco Targets Ther *12*, 4359-4377. 10.2147/OTT.S193507.
53. Chandel, N.S., McClintock, D.S., Feliciano, C.E., Wood, T.M., Melendez, J.A., Rodriguez, A.M., and Schumacker, P.T. (2000). Reactive oxygen species generated at mitochondrial complex III stabilize hypoxia-inducible factor-1alpha during hypoxia: a mechanism of O2 sensing. J Biol Chem *275*, 25130-25138. 10.1074/jbc.M001914200.
54. Liu, Y., Cui, Y., Shi, M., Zhang, Q., Wang, Q., and Chen, X. (2014). Deferoxamine promotes MDA-MB-231 cell migration and invasion through increased ROS-dependent HIF-1α accumulation. Cell Physiol Biochem *33*, 1036-1046. 10.1159/000358674.
55. Dixon, S.J., Lemberg, K.M., Lamprecht, M.R., Skouta, R., Zaitsev, E.M., Gleason, C.E., Patel, D.N., Bauer, A.J., Cantley, A.M., Yang, W.S., et al. (2012). Ferroptosis: an iron-dependent form of nonapoptotic cell death. Cell *149*, 1060-1072. 10.1016/j.cell.2012.03.042.

1046 56. Weymar, G.H.J., Bar-On, Y., Oliveira, T.Y., Gaebler, C., Ramos, V., Hartweger, H.,
1047 Breton, G., Caskey, M., Cohn, L.B., Jankovic, M., and Nussenzweig, M.C. (2022).
1048 Distinct gene expression by expanded clones of quiescent memory CD4(+) T cells
1049 harboring intact latent HIV-1 proviruses. Cell Rep *40*, 111311.
1050 10.1016/j.celrep.2022.111311.
1051 57. Schwartz, O., Maréchal, V., Le Gall, S., Lemonnier, F., and Heard, J.M. (1996).
1052 Endocytosis of major histocompatibility complex class I molecules is induced by the HIV-
1053 1 Nef protein. Nat Med *2*, 338-342. 10.1038/nm0396-338.
1054 58. Herrera, A., and Jones, R.B. (2023). Whack-a-virus: HIV-specific T cells play an
1055 exhausting game. Cell Host Microbe *31*, 1427-1430. 10.1016/j.chom.2023.08.013.
1056 59. Jiang, L., Wang, Y.J., Zhao, J., Uehara, M., Hou, Q., Kasinath, V., Ichimura, T., Banouni,
1057 N., Dai, L., Li, X., et al. (2020). Direct Tumor Killing and Immunotherapy through Anti-
1058 SerpinB9 Therapy. Cell *183*, 1219-1233.e1218. 10.1016/j.cell.2020.10.045.
1059 60. An, X., Yu, W., Liu, J., Tang, D., Yang, L., and Chen, X. (2024). Oxidative cell death in
1060 cancer: mechanisms and therapeutic opportunities. Cell Death Dis *15*, 556.
1061 10.1038/s41419-024-06939-5.
1062 61. Fiorillo, M., Lamb, R., Tanowitz, H.B., Mutti, L., Krstic-Demonacos, M., Cappello, A.R.,
1063 Martinez-Outschoorn, U.E., Sotgia, F., and Lisanti, M.P. (2016). Repurposing
1064 atovaquone: targeting mitochondrial complex III and OXPHOS to eradicate cancer stem
1065 cells. Oncotarget *7*, 34084-34099. 10.18632/oncotarget.9122.
1066 62. Heo, J.R., Kim, S.M., Hwang, K.A., Kang, J.H., and Choi, K.C. (2018). Resveratrol
1067 induced reactive oxygen species and endoplasmic reticulum stress-mediated apoptosis,
1068 and cell cycle arrest in the A375SM malignant melanoma cell line. Int J Mol Med *42*,
1069 1427-1435. 10.3892/ijmm.2018.3732.
1070 63. Olmedo, I., Martinez, D., Carrasco-Rojas, J., and Jara, J.A. (2023). Mitochondria in oral
1071 cancer stem cells: Unraveling the potential drug targets for new and old drugs. Life Sci
1072 *331*, 122065. 10.1016/j.lfs.2023.122065.
1073 64. Clayton, K.L., Collins, D.R., Lengieza, J., Ghebremichael, M., Dotiwala, F., Lieberman,
1074 J., and Walker, B.D. (2018). Resistance of HIV-infected macrophages to CD8(+) T
1075 lymphocyte-mediated killing drives activation of the immune system. Nat Immunol *19*,
1076 475-486. 10.1038/s41590-018-0085-3.
1077 65. Hsu, J.C.-C., Laurent-Rolle, M., and Cresswell, P. (2021). Translational regulation of
1078 viral RNA in the type I interferon response. Current Research in Virological Science *2*,
1079 100012. https://doi.org/10.1016/j.crviro.2021.100012.
1080 66. Su, X., Yu, Y., Zhong, Y., Giannopoulou, E.G., Hu, X., Liu, H., Cross, J.R., Ratsch, G.,
1081 Rice, C.M., and Ivashkiv, L.B. (2015). Interferon-gamma regulates cellular metabolism
1082 and mRNA translation to potentiate macrophage activation. Nat Immunol *16*, 838-849.
1083 10.1038/ni.3205.
1084 67. Cristofoletti, C., Bresin, A., Picozza, M., Picchio, M.C., Monzo, F., Helmer Citterich, M.,
1085 Passarelli, F., Frezzolini, A., Scala, E., Monopoli, A., et al. (2019). Blood and skin-
1086 derived Sezary cells: differences in proliferation-index, activation of PI3K/AKT/mTORC1
1087 pathway and its prognostic relevance. Leukemia *33*, 1231-1242. 10.1038/s41375-018-
1088 0305-8.
1089 68. Korsunsky, I., Millard, N., Fan, J., Slowikowski, K., Zhang, F., Wei, K., Baglaenko, Y.,
1090 Brenner, M., Loh, P.R., and Raychaudhuri, S. (2019). Fast, sensitive and accurate
1091 integration of single-cell data with Harmony. Nat Methods *16*, 1289-1296.
1092 10.1038/s41592-019-0619-0.
1093

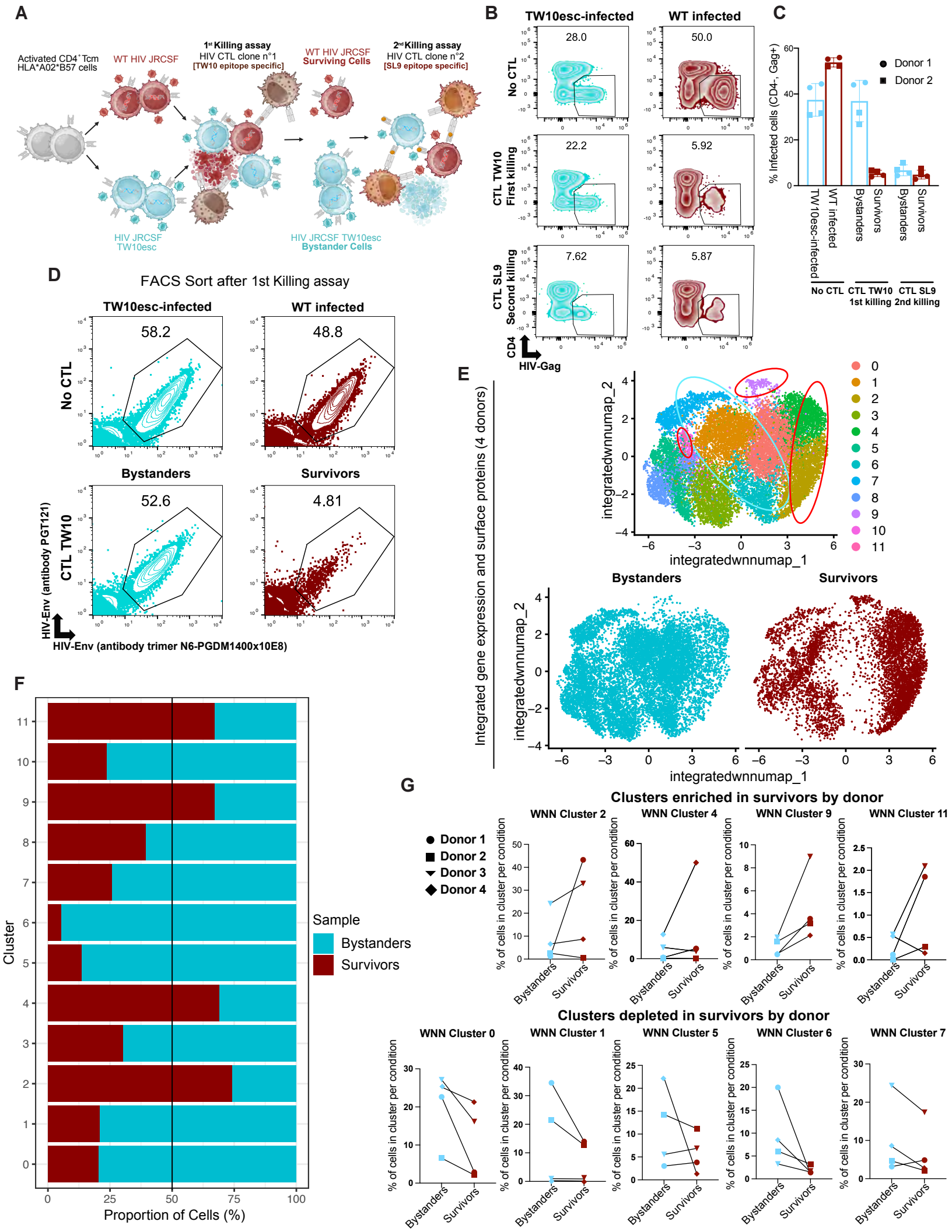
A
Activated CD4+ Tcm
HLA*A02*B57 cells
WT HIV JRCSF
1st Killing assay
HIV CTL clone n°1
[TW10 epitope specific]
WT HIV JRCSF
Surviving Cells
2nd Killing assay
HIV CTL clone n°2
[SL9 epitope specific]
HIV JRCSF
TW10esc
HIV JRCSF TW10esc
Bystander Cells
B
TW10esc-infected
WT infected
No CTL
CTL TW10
First killing
CTL SL9
Second killing
28.0
50.0
22.2
5.92
7.62
5.87
CD4
HIV-Gag
C
% Infected cells (CD4-, Gag+)
Donor 1
Donor 2
TW10esc-infected
WT infected
Bystanders
Survivors
Bystanders
Survivors
No CTL
CTL TW10
1st killing
CTL SL9
2nd killing
D
FACS Sort after 1st Killing assay
TW10esc-infected
WT infected
Bystanders
Survivors
58.2
48.8
52.6
4.81
No CTL
CTL TW10
HIV-Env (antibody PGT121)
HIV-Env (antibody trimer N6-PGDM1400x10E8)
E
Integrated gene expression and surface proteins (4 donors)
integratedwnnumap_1
integratedwnnumap_2
Bystanders
Survivors
F
Cluster
Proportion of Cells (%)
Sample
Bystanders
Survivors
G
Clusters enriched in survivors by donor
WNN Cluster 2
WNN Cluster 4
WNN Cluster 9
WNN Cluster 11
Donor 1
Donor 2
Donor 3
Donor 4
% of cells in cluster per condition
Bystanders
Survivors
Clusters depleted in survivors by donor
WNN Cluster 0
WNN Cluster 1
WNN Cluster 5
WNN Cluster 6
WNN Cluster 7

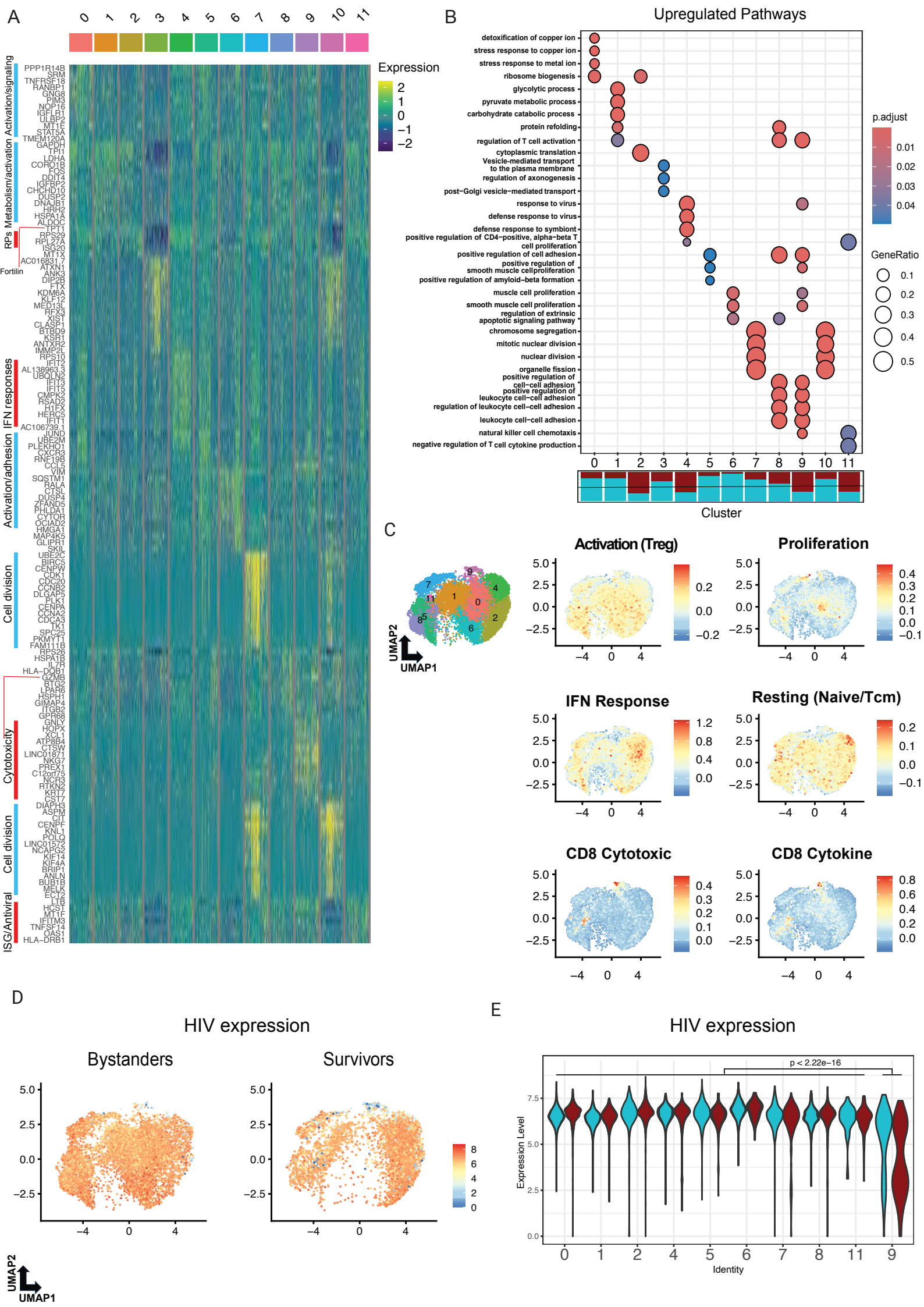
A
0 1 2 3 4 5 6 7 8 9 10 11
Expression
2
1
0
−1
−2
Activation/signaling
Metabolism/activation
RPs
Fortilin
IFN responses
Activation/adhesion
Cell division
Cytotoxicity
Cell division
ISG/Antiviral
PPP1R14B
SRM
TNFRSF18
RANBP1
GNG8
PIM3
NOP16
IGFLR1
ULBP2
MT1E
STAT5A
TMEM120A
GAPDH
TPI1
LDHA
CORO1B
FOS
DDIT4
IGFBP2
CHCHD10
DUSP2
DNAJB1
HRH2
HSPA1A
ALDOC
TPT1
RPS29
RPL27A
ISG20
MT1X
AC016831.7
ATXN1
ANK3
DIP2B
FTX
KDM6A
KLF12
MED13L
RFX3
XIST
CLASP1
BTBD9
KSR1
ANTXR2
IMMP2L
RPS10
IFIT2
AL138963.3
UBQLN2
IFIT3
IFI15
CMPK2
RSAD2
H1FX
HERC5
IFI11
AC106739.1
JUND
UBE2M
PLEKHO1
CXCR3
RNF19B
CCL5
VIM
SQSTM1
RALA
CTSL
DUSP4
ZFAND5
PHLDA1
CYTOR
OCIAD2
HMGA1
MAP4K5
GLIPR1
SKIL
UBE2C
BIRC5
CENPW
CDK1
CDC20
CCNB2
DLGAP5
PLK1
CENPA
CCNA2
CDCA3
TK1
SPC25
PKMYT1
FAM111B
RPS26
HSPA1B
IL7R
HLA−DQB1
GZMB
BTG2
LPAR6
HSPH1
GIMAP4
ITGB2
GPR68
GNLY
HOPX
XCL1
ATP8B4
CTSW
LINC01871
NKG7
PREX1
C12orf75
NCR3
RTKN2
KRT7
CST7
DIAPH3
ASPM
CIT
CENPF
KNL1
POLQ
LINC01572
NCAPG2
KIF14
KIF4A
BRIP1
ANLN
BUB1B
MELK
ECT2
LTB
HCST
MT1F
IFITM3
TNFSF14
OAS1
HLA−DRB1
B
Upregulated Pathways
detoxification of copper ion
stress response to copper ion
stress response to metal ion
ribosome biogenesis
glycolytic process
pyruvate metabolic process
carbohydrate catabolic process
protein refolding
regulation of T cell activation
cytoplasmic translation
Vesicle-mediated transport to the plasma membrane
regulation of axonogenesis
post−Golgi vesicle−mediated transport
response to virus
defense response to virus
defense response to symbiont
positive regulation of CD4−positive, alpha−beta T cell proliferation
positive regulation of cell adhesion
positive regulation of smooth muscle cellproliferation
positive regulation of amyloid−beta formation
muscle cell proliferation
smooth muscle cell proliferation
regulation of extrinsic apoptotic signaling pathway
chromosome segregation
mitotic nuclear division
nuclear division
organelle fission
positive regulation of cell−cell adhesion
positive regulation of leukocyte cell−cell adhesion
regulation of leukocyte cell−cell adhesion
leukocyte cell−cell adhesion
natural killer cell chemotaxis
negative regulation of T cell cytokine production
0 1 2 3 4 5 6 7 8 9 10 11
Cluster
p.adjust
0.01
0.02
0.03
0.04
GeneRatio
0.1
0.2
0.3
0.4
0.5
C
UMAP2
UMAP1
Activation (Treg)
Proliferation
IFN Response
Resting (Naive/Tcm)
CD8 Cytotoxic
CD8 Cytokine
D
HIV expression
Bystanders
Survivors
UMAP2
UMAP1
E
HIV expression
p < 2.22e−16
Expression Level
Identity
0 1 2 4 5 6 7 8 11 9

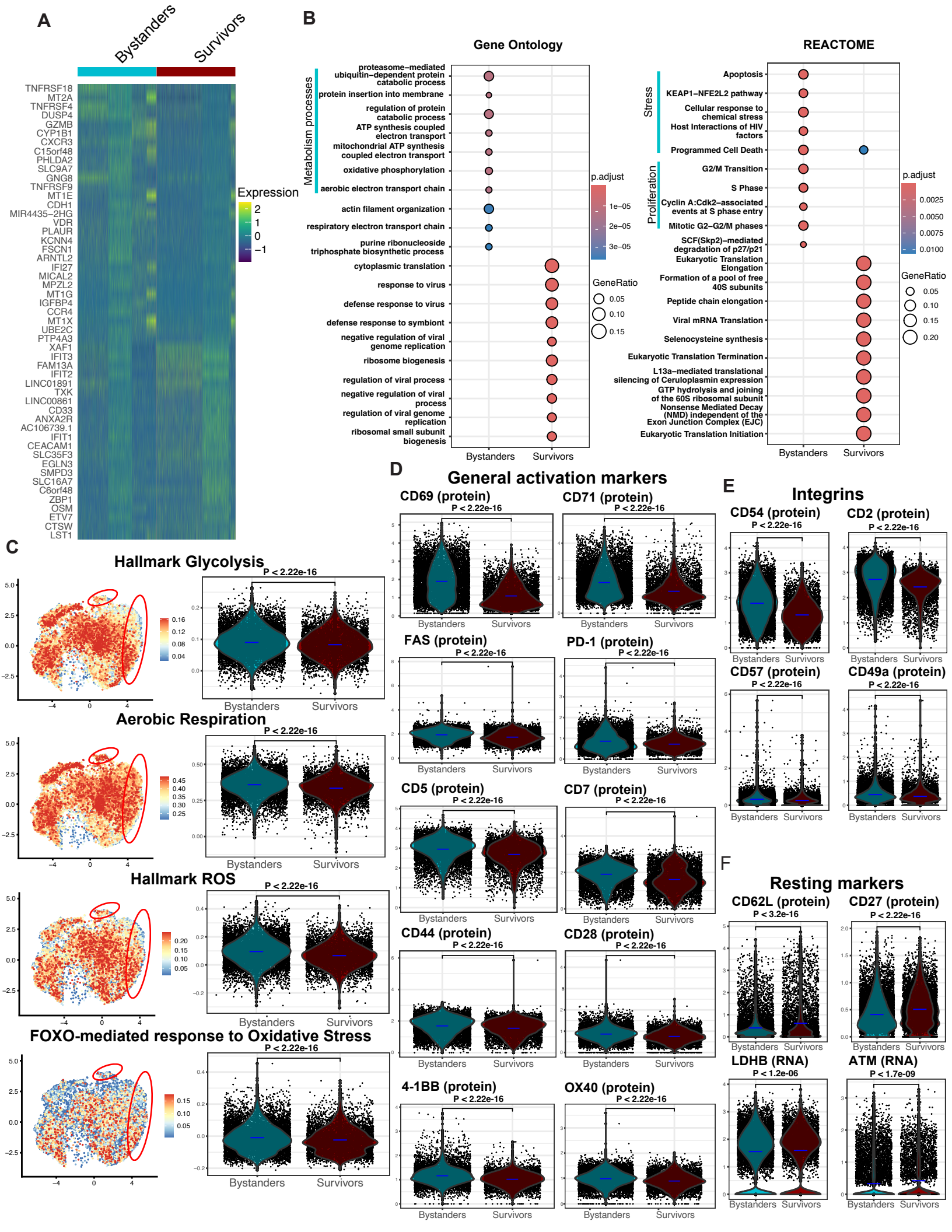
A
Bystanders
Survivors
TNFRSF18
MT2A
TNFRSF4
DUSP4
GZMB
CYP1B1
CXCR3
C15orf48
PHLDA2
SLC9A7
GNG8
TNFRSF9
MT1E
CDH1
MIR4435-2HG
VDR
PLAUR
KCNN4
FSCN1
ARNTL2
IFI27
MICAL2
MPZL2
MT1G
IGFBP4
CCR4
MT1X
UBE2C
PTP4A3
XAF1
IFIT3
FAM13A
IFIT2
LINC01891
TXK
LINC00861
CD33
ANXA2R
AC106739.1
IFIT1
CEACAM1
SLC35F3
EGLN3
SMPD3
SLC16A7
C6orf48
ZBP1
OSM
ETV7
CTSW
LST1
Expression
2
1
0
−1
B
Gene Ontology
Metabolism processes
proteasome−mediated ubiquitin−dependent protein catabolic process
protein insertion into membrane
regulation of protein catabolic process
ATP synthesis coupled electron transport
mitochondrial ATP synthesis coupled electron transport
oxidative phosphorylation
aerobic electron transport chain
actin filament organization
respiratory electron transport chain
purine ribonucleoside triphosphate biosynthetic process
cytoplasmic translation
response to virus
defense response to virus
defense response to symbiont
negative regulation of viral genome replication
ribosome biogenesis
regulation of viral process
negative regulation of viral process
regulation of viral genome replication
ribosomal small subunit biogenesis
Bystanders
Survivors
p.adjust
1e−05
2e−05
3e−05
GeneRatio
0.05
0.10
0.15
REACTOME
Stress
Apoptosis
KEAP1−NFE2L2 pathway
Cellular response to chemical stress
Host Interactions of HIV factors
Programmed Cell Death
Proliferation
G2/M Transition
S Phase
Cyclin A:Cdk2−associated events at S phase entry
Mitotic G2−G2/M phases
SCF(Skp2)−mediated degradation of p27/p21
Eukaryotic Translation Elongation
Formation of a pool of free 40S subunits
Peptide chain elongation
Viral mRNA Translation
Selenocysteine synthesis
Eukaryotic Translation Termination
L13a−mediated translational silencing of Ceruloplasmin expression
GTP hydrolysis and joining of the 60S ribosomal subunit
Nonsense Mediated Decay (NMD) independent of the Exon Junction Complex (EJC)
Eukaryotic Translation Initiation
Bystanders
Survivors
p.adjust
0.0025
0.0050
0.0075
0.0100
GeneRatio
0.05
0.10
0.15
0.20
C
Hallmark Glycolysis
P < 2.22e-16
Bystanders
Survivors
Aerobic Respiration
P < 2.22e-16
Bystanders
Survivors
Hallmark ROS
P < 2.22e-16
Bystanders
Survivors
FOXO-mediated response to Oxidative Stress
P < 2.22e-16
Bystanders
Survivors
D
General activation markers
CD69 (protein)
P < 2.22e-16
CD71 (protein)
P < 2.22e-16
FAS (protein)
P < 2.22e-16
PD-1 (protein)
P < 2.22e-16
CD5 (protein)
P < 2.22e-16
CD7 (protein)
P < 2.22e-16
CD44 (protein)
P < 2.22e-16
CD28 (protein)
P < 2.22e-16
4-1BB (protein)
P < 2.22e-16
OX40 (protein)
P < 2.22e-16
Bystanders
Survivors
E
Integrins
CD54 (protein)
P < 2.22e-16
CD2 (protein)
P < 2.22e-16
CD57 (protein)
P < 2.22e-16
CD49a (protein)
P < 2.22e-16
Bystanders
Survivors
F
Resting markers
CD62L (protein)
P < 3.2e-16
CD27 (protein)
P < 2.22e-16
LDHB (RNA)
P < 1.2e-06
ATM (RNA)
P < 1.7e-09
Bystanders
Survivors

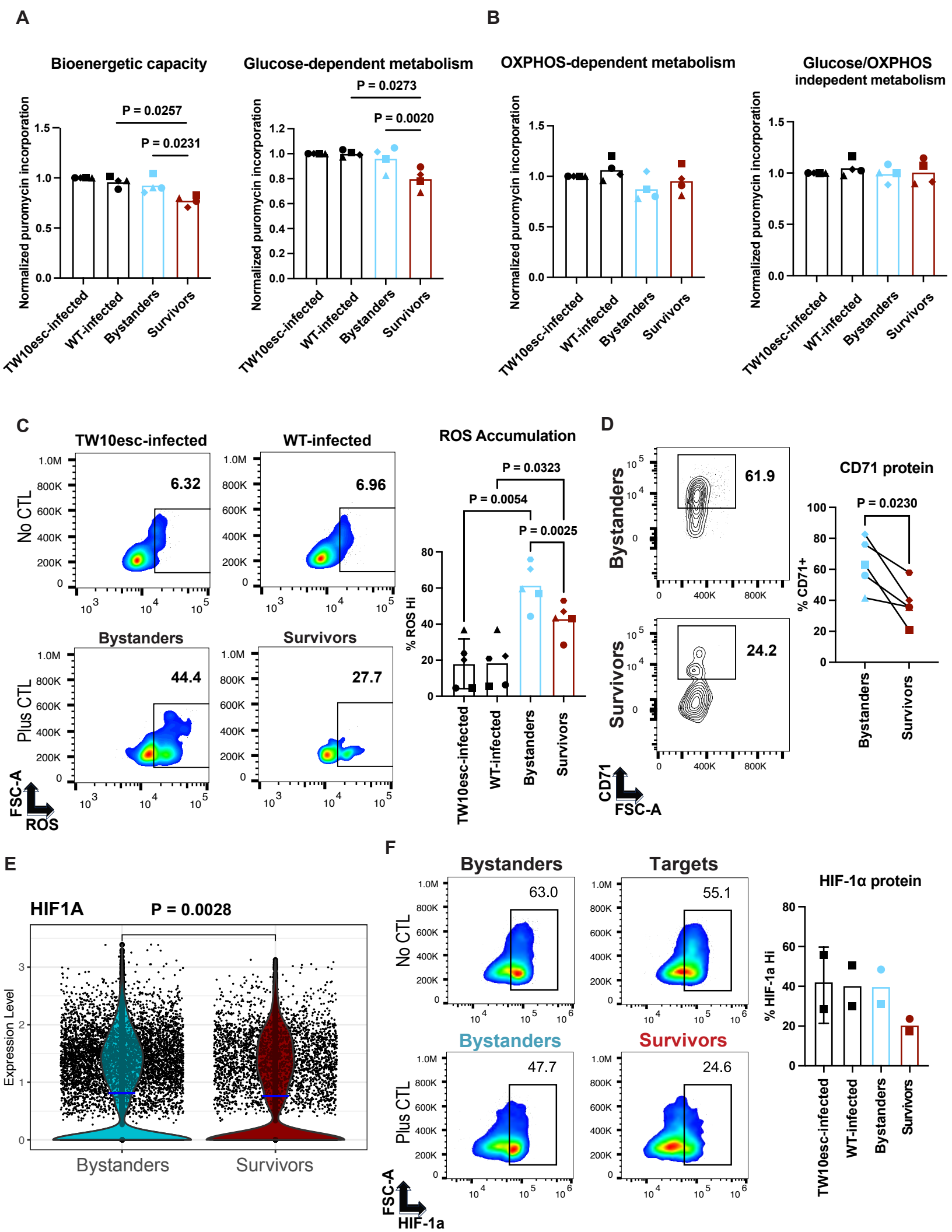
A
Bioenergetic capacity
Glucose-dependent metabolism
P = 0.0257
P = 0.0231
P = 0.0273
P = 0.0020
Normalized puromycin incorporation
TW10esc-infected
WT-infected
Bystanders
Survivors
B
OXPHOS-dependent metabolism
Glucose/OXPHOS indepedent metabolism
C
TW10esc-infected
WT-infected
Bystanders
Survivors
No CTL
Plus CTL
6.32
6.96
44.4
27.7
FSC-A
ROS
ROS Accumulation
P = 0.0323
P = 0.0054
P = 0.0025
% ROS Hi
D
61.9
24.2
CD71
FSC-A
CD71 protein
P = 0.0230
% CD71+
E
HIF1A
P = 0.0028
Expression Level
F
63.0
55.1
47.7
24.6
HIF-1a
HIF-1α protein
% HIF-1a Hi

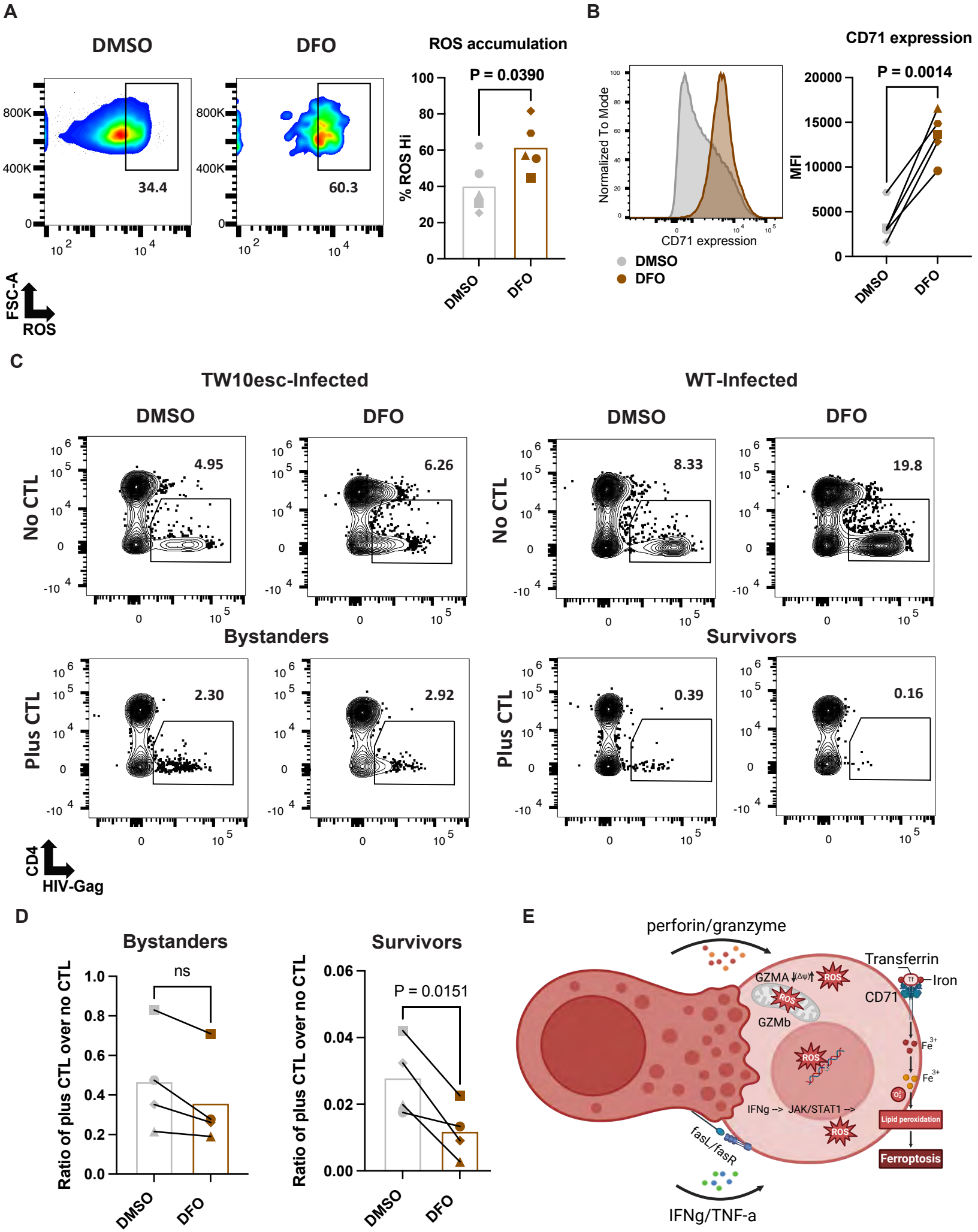
A
DMSO
DFO
ROS accumulation
800K
400K
0
34.4
60.3
P = 0.0390
% ROS Hi
100
80
60
40
20
0
DMSO
DFO
FSC-A
ROS
B
CD71 expression
Normalized To Mode
CD71 expression
DMSO
DFO
P = 0.0014
MFI
20000
15000
10000
5000
0
DMSO
DFO
C
TW10esc-Infected
WT-Infected
DMSO
DFO
DMSO
DFO
No CTL
4.95
6.26
8.33
19.8
Bystanders
Survivors
Plus CTL
2.30
2.92
0.39
0.16
CD4
HIV-Gag
D
Bystanders
Survivors
ns
P = 0.0151
Ratio of plus CTL over no CTL
1.0
0.8
0.6
0.4
0.2
0.0
0.06
0.04
0.02
0.00
DMSO
DFO
E
perforin/granzyme
Transferrin
Iron
CD71
GZMA
GZMb
ROS
IFNg --> JAK/STAT1 -->
fasL/fasR
Lipid peroxidation
Ferroptosis
IFNg/TNF-a

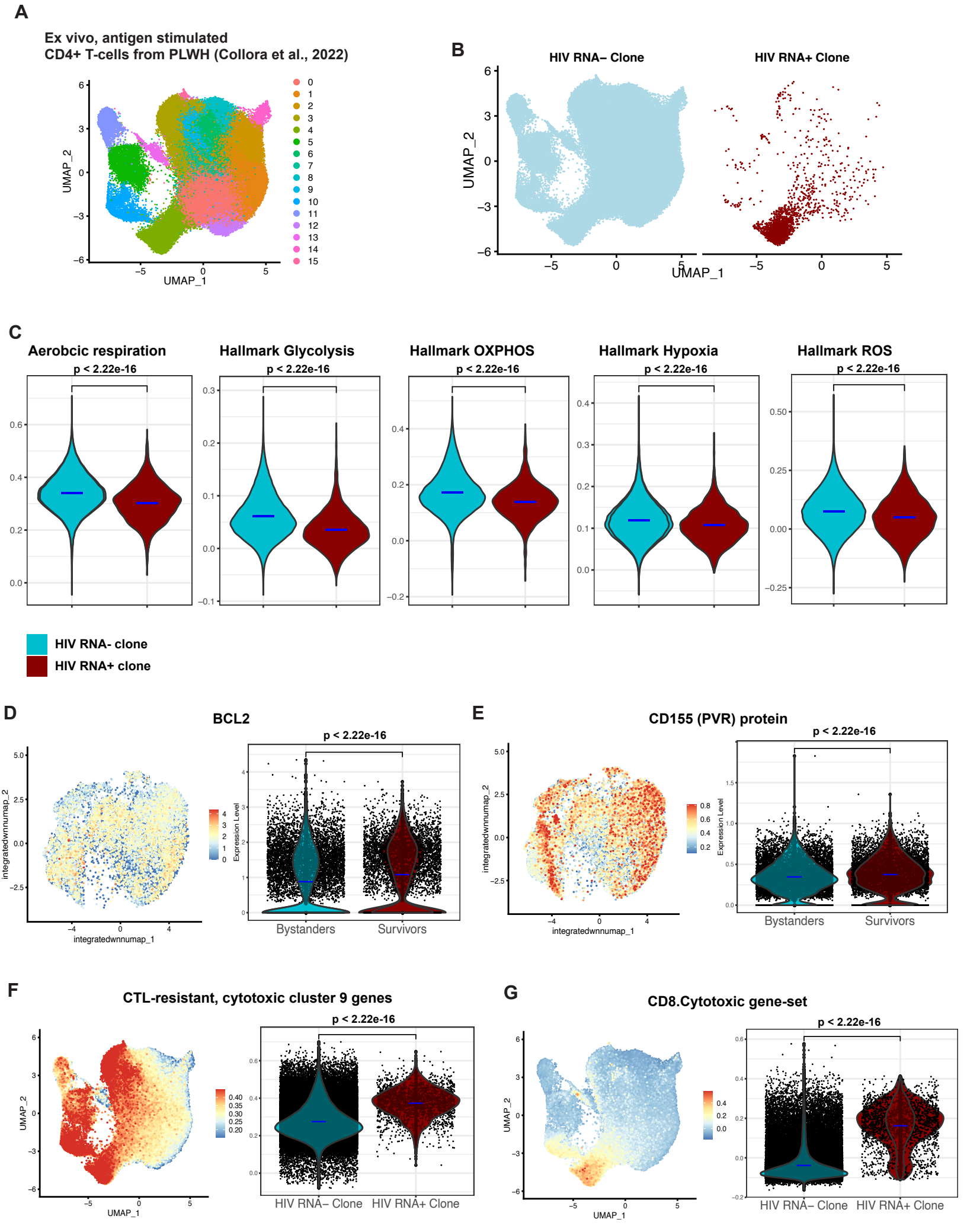
A
Ex vivo, antigen stimulated
CD4+ T-cells from PLWH (Collora et al., 2022)
UMAP_2
UMAP_1
0
1
2
3
4
5
6
7
8
9
10
11
12
13
14
15
B
HIV RNA– Clone
HIV RNA+ Clone
UMAP_2
UMAP_1
C
Aerobcic respiration
Hallmark Glycolysis
Hallmark OXPHOS
Hallmark Hypoxia
Hallmark ROS
p < 2.22e-16
HIV RNA- clone
HIV RNA+ clone
D
BCL2
p < 2.22e-16
integratedwnnumap_2
integratedwnnumap_1
Expression Level
Bystanders
Survivors
E
CD155 (PVR) protein
p < 2.22e-16
integratedwnnumap_2
integratedwnnumap_1
Expression Level
Bystanders
Survivors
F
CTL-resistant, cytotoxic cluster 9 genes
p < 2.22e-16
UMAP_2
UMAP_1
HIV RNA– Clone
HIV RNA+ Clone
G
CD8.Cytotoxic gene-set
p < 2.22e-16
UMAP_2
UMAP_1
HIV RNA– Clone
HIV RNA+ Clone